This is a preprint, the final version is subject to change, of the American Mineralogist (MSA)
Cite as Authors (Year) Title. American Mineralogist, in press.
DOI: https://doi.org/10.2138/am-2019-6708

Revision 1

'Kamchatite' diamond aggregate from northern Kamchatka, Russia: New find of diamond formed by gas phase condensation or chemical vapor deposition

Felix V. Kaminsky [a,*], Richard Wirth [b], Leonid P. Anikin [c], Anya Schreiber [b]

[a] *KM Diamond Exploration Ltd., West Vancouver, BC, V7S 3J1, Canada*

[b] *Helmholtz Centre Potsdam, GFZ German Research Center for Geosciences, Telegrafenberg,C120, D-14473 Potsdam, Germany*

[c] *Institute of Volcanology and Seismology, Russian Academy of Sciences, Petropavlovsk–Kamchatskii, 683006, Russia*

Highlights

- Polycrystalline diamond identified in northern Kamchatka;
- Diamond microcrystals are cemented with tilleyite, SiC, Fe-Ni-Mn silicides, native Si, graphite, calcite, and amorphous material;
- The assemblage was formed via gas phase condensation or CVD.

Absract

* Corresponding author. Tel +1 604 925 8755.
E-mail address: felixvkaminsky@aol.com

A series of polycrystalline diamond grains were found within the Valizhgen Peninsula in Koryakia, northern Kamchatka, Russia. A grain from the Aynyn River area is studied in detail with TEM. Diamond crystallites, 2-40 μm in size are twinned and have high dislocation density. They are cemented with tilleyite $Ca_5(Si_2O_7)(CO_3)_2$, SiC, Fe-Ni-Mn-Cr silicides, native silicon, graphite, calcite, and amorphous material. Among SiC grains, three polymorphs were discriminated: hexagonal 4H and 6H and cubic C3 (β-SiC). Silicides have variable stoichiometry with (Fe,Ni,Mn,Cr)/Si = 0.505-1.925. Native silicon is an open-framework allotrope of silicon S_{24}, which has been observed, to date, as a synthetic phase only; this is a new natural mineral phase. Three types of amorphous material were distinguished: a Ca-Si-C-O material, similar in composition to tilleyite; amorphous carbon in contact with diamond, which includes particles of crystalline graphite; and amorphous SiO_2. No regularity in the distribution of the amorphous material was observed. In the studied aggregate, diamond crystallites and moissanite are intensively twinned, which is characteristic for these minerals formed by gas phase condensation or chemical vapor deposition (CVD) processes. The synthetic analogs of all other cementing compounds (β-SiC, silicides and native silicon) are typical products of CVD processes. This confirms the earlier suggested CVD mechanism for the formation of Avacha diamond aggregates. Both Avacha and Aynyn diamond aggregates are related not to 'classic' diamond locations within stable cratons, but to areas of active and Holocene volcanic belts. The studied diamond aggregates from Aynyn and Avacha, by their mineralogical features, and by their origin during the course of volcanic eruptions via a gas phase condensation or CVD mechanism may be considered as a new variety of polycrystalline diamond and may be called 'kamchatite'. Kamchatite extends the number of unusual diamond localities. It increases the potential sources of diamond and indicates the polygenetic character of diamond.

Keywords: diamond, kamchatite, Kamchatka, SiC, tilleyite, silicide, native silicon, CVD

1. Introduction

In recent decades the number of finds of diamond in uncommon tectonic settings and of unusual appearance has increased (Kaminsky, 2007; Golovko and Kaminsky, 2010). Of particular interest, in this respect, is the territory of Kamchatka, Russia, where monocrystalline diamond and polycrystalline diamond aggregates were identified in various volcanic and ultramafic rocks (Kutyev and Kutyeva, 1975; Shilo et al., 1979; Baikov et al., 1995; Gorshkov et al., 1995; Seliverstov, 2009). A summary of these finds was presented recently by Kaminsky et al. (2016) along with the results of a study of uncommon, 'carbonado-like' diamond aggregates from the lavas of the active Avacha volcano.

These finds demonstrate that diamond is a mineral, which may originate not only at static or dynamic high pressure-temperature (*P*-*T*) conditions, but also during the course of near-atmospheric processes of gas phase condensation or chemical vapor deposition (CVD) (Kaminsky et al., 2016). The number of such finds, confirming the idea of the polygenesis of diamond, increases. In this work we continue studying unusual diamond aggregates from Kamchatka and describe another find of a diamond aggregate in northern Kamchatka, formed, most likely, like the Avacha diamond aggregates, during the course of near-atmospheric CVD processes.

2. Geological setting of the diamond microcrystalline aggregate

In the 1980s a series of carbonado-like diamond grains were found within the Valizhgen Peninsula in Koryakia, northern Kamchatka, Russia (Fig. 1). The area is composed of Paleozoic silicic-tuffaceous rocks, slightly deformed Upper Jurassic-Lower Cretaceous terrigenous units, and ultramafic rocks, which belong to the Talovo-Pekul'nei ophiolite belt comprising ophiolites of various ages, peridotites and various gabbroic rocks. More than a hundred isolated ultramafic rock bodies, scattered over the Valizhgen rise, are suggested to be fragments of a large, low-angle plate-shaped body composed of several sheets. The ultramafic bodies always have tectonic contacts with host arkose sandstones and siltstones; at the

flanks of the Valizhgen rise they are overlain by terrigenous Upper Cretaceous deposits. Chromite ore mineralization is associated with the dunite lenses (Osipenko et al., 2002). F.Sh. Kutyev (pers. comm.), during the course of his sampling the Valizhgen area, indentified several fresh (3-7 thousand year old) basaltic cones within the Aynyn River valley.

More than 40 grains of diamond aggregate were found in 1983-1988 in eight 20-litre panning samples, collected from recent alluvium from the following rivers: Ilistaya (15 grains in two samples), Gorelaya (20 grains in two samples), Dlinnaya (two grains in one sample) and Smyatii Creek (eight grains in two samples). Later, one of the authors (LPA) identified a carbonado-like grain, Ayn-3, in a sample from the Aynyn River, the left tributary of the Talovka River (Fig. 1).

3. Sample characteristics and methods

The studied microcrystalline diamond aggregate Ayn-3 is of elongated-rounded shape, ~1 mm in size. Diamond crystallites occupy 52-55 vol.% of the aggregate; they are cemented with a nanocrystalline aggregate of various minerals and amorphous material (Fig. 2).

Five electron-transparent foils (##4975, 4976, 5312, 5316B and 5317C) with typical dimensions of 15 × 8 × 0.15 μm have been prepared applying focused ion beam (FIB) sample preparation. Details of foil preparation are given in Wirth (2004, 2009). Transmission electron microscopy (TEM) was performed using a Tecnai F20 X-Twin microscope, operated at 200 kV with a Schottky emitter as electron source (FEG). The TEM is equipped with an EDAX X-Ray analyzer with ultra-thin window, a Fishione high-angle annular dark-field (HAADF) detector and a Gatan imaging filter (Tridiem) for electron energy-loss spectroscopy and energy filtered imaging. HAADF images were collected with a camera length of 330mm displaying diffraction contrast plus Z-contrast or with a camera length of 75 mm which shows Z-contrast only. Usually, nanophases were identified acquiring high-resolution lattice fringe images with a very short acquisition time (0.6 seconds) to avoid decomposition during exposure to the electron beam. The calculated diffraction patterns from high-resolution images were used to measure *d*-spacing and

angles between the adjacent planes. A comparison of the observed data with calculated data from known structures (literature data) allows for the identification of phases present. The chemical composition of the phases was always measured in the scanning transmission mode (STEM) thus avoiding significant mass loss during data acquisition. Acquisition time was 60 or 120 seconds. Data evaluation occurred using the TIA software package of the microscope.

4. Results

All foils show diamond crystallites, cemented with tilleyite, SiC, Fe-Ni-Mn silicides, native silicon, graphite, calcite, and amorphous material. The peculiar features of this sample, compared with other known diamond aggregates (boart, framesite, carbonado) is that diamond crystallites are not sintered together but are cemented by other phases and/or amorphous material, and that they comprise only a half of the volume of the aggregate (52-55 vol.%).

4.1. Diamond crystallites

Crystallites of diamond are octahedral and, sometimes, irregular grains 2-40 μm in size (Fig. 2b). They are usually intensively twinned after (111) as twin planes (Fig. 3a). Some crystallites show a very high dislocation density so that individual lines cannot be distinguished (Fig. 3b); the others show low or very low dislocation density.

4.2. Cementing matrix

The matrix, cementing the diamond aggregate, comprises almost a half of its volume. It consists of crystalline and amorphous tilleyite, SiC, Fe-Ni-Mn silicides, native silicon, graphite, calcite, and amorphous material (Fig. 4).

Tilleyite $Ca_5(Si_2O_7)(CO_3)_2$ is the major component of the matrix (Fig. 4). In addition to nanocrystals, 40-50 nm in size, amorphous material with a similar composition to tilleyite, occupies the significant part of the matrix (Supplementary Fig. 1). Tilleyite was confirmed by diffraction data from high-resolution images (Supplementary Table 1).

SiC is the second major phase in the groundmass cementing diamond crystallites. It forms small irregular grains, 5-50 nm in size, intergrown with tilleyite (Fig. 4). Three polymorphs were discriminated among them: hexagonal 4H and 6H (usually intensively twinned) and cubic (not twinned in the studied grain). These have been identified from diffraction patterns (FFT) calculated from high-resolution images. The structural data of hexagonal SiC are presented in Supplementary Table 2, and the cubic crystal symmetry of SiC, determined on the base of three diffraction patterns, calculated from high-resolution images (FFT) with three different zone axis orientations, is shown in Supplementary Fig. 2.

Silicides. Irregular and hexagonal crystals of Fe-Ni-Mn-Cr silicides, approximately 100-400 nm in size, are commonly embedded in the tilleyite-SiC matrix or located between diamond crystallites (Fig. 5). Chemical compositions of Fe-Ni-Mn-Cr silicide grains from different foils show great variability with (Fe+Mn+Ni+Cr)/Si atomic ratios from 0.505 to 1.925 (Table 1). Minor admixtures of Ti and Cr also exist. The variations occur not only among different grains but also within a single grain (Table 1 and Supplementary Fig. 3). The compositional variations of the silicides are summarized in Fig. 6.

Several compositional and structural groups of silicides may be distinguished (Fig. 6a). Group 1 comprises the grains with (Fe,Ni,Mn,Cr)/(Si+Ti) = 1.888-1.925, which includes grain #HREM02. This grain, according to its structural characteristics (Supplementary Table 3), has a hexagonal structure with an average stoichiometry of $(Fe,Ni,Mn)_5Si_3$ (Bińczyska et al., 1973) or orthorhombic structure with a stoichiometry, FeNiSi (Landrum et al., 1998); the same structure may be suggested for another grain with similar chemical composition. Group 2 includes the grains with (Fe,Ni,Mn,Cr)/(Si+Ti) = 0.961-1.085, including grain #HREM04. This grain, most likely, has a cubic structure with an average stoichiometry of (Fe,Mn)Si (Aronsson 1958); the same structure is suggested for other grains from the same chemical group. Group 3 includes grains with (Fe,Ni,Mn,Cr)/(Si+Ti) = 0.505-0.605; their supposed stoichiometry

is $(Fe,Ni,Mn,Cr)(Si,Ti)_2$, which may be orthorhombic (Kojima et al., 1990) (Supplementary Table 3). There are also silicides with chemical compositions intermediate between the three groups, such as (Fe,Ni,Mn,Cr)/(Si+Ti) = 1.2 (sample #4976-5), (Fe,Ni,Mn,Cr)/(Si+Ti) = 1.5 (sample #4976-6) and (Fe,Ni,Mn,Cr)/(Si+Ti) = 0.66 (samples ##5317-31, 32). Variable stoichiometries and other structures may be suggested to exist in such silicides. The variations in major cation compositions are more random, occupying almost the entire field in the Fe-Ni-Mn plot (Fig. 6b). This confirms the variable stoichiometry of the investigated, Aynyn Fe-Ni-Mn-Cr silicides.

Native silicon Si_{24}. Several grains of pure native Si^0, 300-600 nm in size, were identified in foil #5312. They occur in a touching association with diamond and silicide (Fig. 7a). The grains are polycrystalline, representing a mosaic of almost equally-oriented nanocrystals, 5-20 nm in size (Fig. 7b). Some crystallites are twinned. The slight misorientation between the individual nanocrystals is documented in smeared-out diffraction spots in the diffraction pattern that cover a larger volume of the crystal including many individual nanocrystals, while singular nanocrystals show sharp diffraction spots (Fig. 7c). The dark-field image, acquired using a (141) reflection of Si^0, shows the entire crystal in a brighter contrast, demonstrating very bright nanocrystals with perfect orientation along the identified zone axis (Fig. 7d). High-resolution HAADF images show individual crystals with a grain size range of only 5–20 nm and with nanoporosity in between (Fig. 7b). The identification of native silicon as Si_{24} is based on diffraction data from high-resolution imaging (FFT) comparing the observed *d*-spacings and angles between adjacent planes with the values calculated based on the structural data given by Kim et al., (2015) (Supplementary Table 4).

Graphite. At a contact of tilleyite-composed Ca-Si-C-O amorphous mass with diamond grains, thin (less than 25 nm) rims of amorphous carbon material with graphite flakes occur (Fig. 4b). High-resolution imagery demonstrates the gradual transformation of amorphous carbon into graphite (Fig. 8).

Calcite associates with amorphous carbon and ***amorphous SiO_2*** within the matrix. It forms angular grains, which are strongly porous (Fig. 9).

178 ***Amorphous matrix***. In addition to mineral phases in the matrix, which cements diamond
179 crystallites, such as tilleyite, SiC, silicides, native silicon, graphite and calcite, the bulk of the matrix is
180 composed of amorphous material. This amorphous material is of variable composition. Three types of
181 amorphous materials were distinguished: a Ca-Si-C-O material, similar in composition to tilleyite
182 $Ca_5(Si_2O_7)(CO_3)_2$ (Fig. 4a); amorphous carbon at a contact with diamond, including particles of
183 crystalline graphite (Figs. 4b and 8); and amorphous SiO_2 (Fig. 9). No regularity in the distribution of the
184 amorphous materials was observed.
185
186 **5. Discussion**
187
188 In our previous publication we described carbonado-like polycrystalline diamond aggregates from
189 the active Avacha volcano in Kamchatka, that were formed via low-*PT* gas phase condensation (chemical
190 vapor deposition, or CVD mechanisms) during the course or shortly after one of the volcanic eruption
191 pulses of the volcano (Kaminsky et al., 2016). Evidence for that conclusion was the intensive twinning in
192 diamond crystallites, the unique set of mineral inclusions in the diamond, and the cementing of diamond
193 crystallites by interstitial amorphous silica with tridymite or β-SiC together with native Si^0, rather than
194 sintering characteristic for carbonado. Similar features were observed for the studied diamond aggregate.
195 Like in the Avacha diamond aggregate and unlike in carbonado, diamond crystallites in the studied
196 Aynyn diamond aggregate are not sintered but cemented with the polymineral aggregate, which includes
197 various amorphous materials. This implies a non-traditional, specific kind of origin for this aggregate.
198 The ***diamond*** crystallites in the studied aggregate, like in the Avacha aggregate, along with high
199 dislocation density, demonstrate intense twinning by {111} twins (Fig. 3a). The twinning mechanism in
200 diamond is characteristic of diamonds grown via the mechanism of CVD (Shechtman et al., 1993;
201 Dischler and Wild, 1998; Butler and Oleynik, 2008).
202 The other mineral phases, cementing diamond, are also low-pressure compounds. ***Tilleyite***
203 $Ca_5(Si_2O_7)(CO_3)_2$, since its discovery in a contact zone of limestones with granodiorite and quartz

monzonite in California (Larsen and Dunham, 1933), was also identified in other calcitic skarns worldwide (e.g., Nockolds and Vincent, 1947; Rubenach and Cuff, 1985; Beard and Drake, 2016) and in Oldoinyo Lengai (Tanzania) natrocarbonatites (Mitchell, 1997). The stability of tilleyite was experimentally determined between 930-970 °C at ~35 MPa of CO_2 and between 870-930 °C at ~20 MPa of CO_2. In the P_{CO2} – T diagram its stability field forms a narrow band lying between the more carbonated calcite + wollastonite assemblage and the less carbonated spurrite (Harker 1959).

Natural ***cubic β-SiC*** was also identified first in shales of the Green River formation, Wyoming, USA, where it was formed as the product of hot volcanic fluids (Regis and Sand, 1958). Later, β-SiC was found in suevites from the Ries meteorite crater, where it is intergrown with diamond and hexagonal H4 moissanite, formed via the CVD mechanism from vaporized carbon-bearing rocks (Hough et al., 1995), and recently (*in situ*, and also in association with 4H moissanite) in recycled aposedimentary carbonatite xenoliths from Neogene basalts in the Dalihu area, Inner Mongolia, China (He et al., 2017). In the diamond aggregate from Avacha, β-SiC is twinned and has a CVD origin (Kaminsky et al., 2016). This allows us to suggest also a relatively low-pressure, CVD mechanism for the β-SiC formation in the studied Aynyn sample.

Hexagonal SiC (moissanite) was considered usually to be a high-pressure mineral (e.g., Kaminsky et al., 1968; Di Pierro et al., 2003). However, Shiryaev and Gaillard (2014) created a thermodynamic model, according to which moissanite may originate not necessarily at high pressures. The association of moissanite with highly reduced phases, such as native Si, various carbides and silicides, may be formed under low pressures at low oxygen fugitivity ($fO_2 \leq$ IW-6). Later Golubkova et al. (2016), analyzing the stability of SiC, demonstrated that it forms, in association with silicides, alloys and native metals, under variable (including low) pressures and low to moderate temperatures from ultra-reduced fluids (fO_2 = IW-6.5 to -7.5). Recently, this hypothesis was confirmed by finds of *in situ* moissanite in low-pressure formations of Neogene and Miocene basalts in China and Israel (Dobrzhinetskaya et al., 2018). In Inner Mongolia, China, hexagonal moissanite associate with cubic β-SiC (He et al., 2017); in Miocene alkali-

basaltic tuffs in Israel moissanite has inclusions of native silicon and metal silicides, where these minerals were supposedly formed from highly reduced fluids (H_2O-CH_4-H_2-C_2H_6) within a shallow magma reservoir (Dobrzhinetskaya et al., 2018). The moissanite grains studied in this work are strongly twinned, implying their low-pressure origin, most likely via the CVD mechanism. SiC was recently described as a vapor condensation product after a lightning strike (Ballhaus et al., 2017)

Metal (Fe-Ni-Mn-Cr) silicides identified in this work are similar in their compositions to Group 2 Mn-Ni-Si-Fe alloys from inclusions in diamond aggregate from the Avacha active volcano, reported in our previous work (Kaminsky et al., 2016); both are silicides. Silicides are very rare natural minerals. Among them, various iron (as well as Fe-Ni and Fe-Ti) silicides predominate, such as gupeiite Fe_3Si, suessite $(Fe,Ni)_3Si$, hapkeite Fe_2Si, naquite FeSi, linzhiite $FeSi_2$, luobusaite Fe_3Si_7, zangboite $TiFeSi_2$ and xifengite Fe_5Si_3 (Mindat: http://www.mindat.org). Their stoichiometry varies widely, from Me/Si = 3 to 0.42. Most of them are identified in meteorites and cosmic dust, such as suessite and hapkeite (Anand et al., 2004; Rietmeijer et al., 2008), as well as the manganese silicide, brownleeite MnSi (Nakamura-Messenger et al., 2010); some are known from terrestrial formations, frequently as inclusions in moissanite along with native Si^0 (Shiryaev et al., 2011).

Most finds of terrestrial Fe-silicides are made in chromitites from the Luobusa ultramafic massif, Tibet, China. These are luobusaite Fe_3Si_7, zangboite $TiFeSi_2$, naquite FeSi and linzhiite $FeSi_2$ (Hu, 1999; Bai et al., 2000, 2006; Li et al.,, 2009, 2012; Shi et al., 2012). Prior to the latter two Fe-silicides being identified in the Luobusa chromitites, they were initially discovered in the 1960s in Miocene sandstones of the Poltavskaya series and placer deposits in the northern Azov area, Donetsk Republic, and named 'fersilicite' and 'ferdisilicite', respectively (Gevorkyan, 1969; Gevorkyan et al., 1969; Fleishner, 1969); and zangboite was met in glassy fulgurites from Michigan, USA (Essene and Fisher 1986). In the 1980s, the Mn-Fe silicides, mavlyanovite Mn_5Si_3 and unnamed $(Mn,Fe)_7Si_2$ were found in association with moissanite and graphite as inclusions in volcanic glass near Volnovakha, Priazovye, Donetsk Republic (Tatarintsev et al., 1990). Such volcanic material may be the source of the silicides found in that area earlier. Silicides were also reported from carbonate rocks (Novoselova and Bagdasarov,1979; Tishchenko

et al., 2016) and as inclusions in moissanite from Yakutian kimberlites (Marshintsev et al., 1967; Pankov and Spetsius, 1989) and other rocks (Di Pierro et al., 2003). Recently, gupeiite, FeTiSi and FeTi(Si,P), in association with khamrabaevite TiC, FeTi and other highly reduced mineral phases, were identified in Cretaceous basaltic pyroclastic rocks exposed on Mount Carmel near Haifa, northern Israel (Griffin et al., 2016).

Three Fe-silicides, possibly corresponding in composition to suessite, hapkeite and xifengite, were found within Co-Mn crust dredged at the depth of 2486 m from a guyot in the central Pacific, at 19N and 175W (Mindat: http://www.mindat.org). A new, palladium silicide (palladosilicide) Pd_2Si was identified in chromitites of the Bushveld complex in the North West Province, South Africa and of the Kapalagulu intrusion, western Tanzania (Cabri et al., 2015). Recently Dobrzhinetskaya et al. (2018) found Fe-Ni and V-Ti silicides included in moissanite from Miocene tuff deposits located within Yizre'el Valley of Qishon River, Israel. They have compositions: $(Fe,Ni)_3Si_2$ and $(Fe,Ni,V,Zr)_3Ti_2Si_4$ (both orthorhombic) and V_2TiSi_5 (cubic).

The conditions of the formation of terrestrial silicides are debatable. The origin of silicides from the Luobusa chromitites was attributed to the deep mantle (Li et al., 2009, 2012). In contrast, Cabri et al. (2015) consider palladosilicide formation as a result of magmatic crystallization. In any case, the formation of silicides, particularly in association with moissanite and native metals, requires an extremely low oxygen fugacity, up to fO_2 = IW-10 to -12 (Griffin et al., 2016). The silicides from the studied diamond aggregate have very variable compositions even within a single grain (Table 1 and Supplementary Fig. 3). This implies unstable, disequilibrium conditions during the course of their origin and disagrees with stable, high-*PT* model of their formation (Li et al., 2009, 2012). The formation of the studied Fe-Ni-Mn-Cr silicides in the diamond aggregate most likely is similar to common low-*PT* synthesis of artificial silicides via vacuum evaporation, sputtering, and chemical vapor deposition (e.g., Nicolet and Lau, 1983).

Native silicon Si^0 is also a very rare natural mineral. In the terrestrial environment, it was identified in serpentinites after ultramafic rocks (Bird and Weathers, 1975; Novgorodova et al., 1989) and chromitites

of Tibet, China (Hu, 1999; Bai et al., 2000; Trumbull et al., 2009; Zhang et al., 2016) and the Polar Urals, Russia (Yang et al., 2015), in kimberlites of Siberia and China (Marshintsev et al., 1967; Pankov and Spetsius, 1989; Leung et al., 1990), in fulgirites (Essene and Fisher, 1986) and fumaroles of Kamchatka and Kuril Islands, Russia (Korzhinskii et al., 1996), and in other rocks (Di Pierro et al., 2003). In all cases, native silicon is associated with silicides, moissanite, native iron, graphite, i.e., in highly reduced conditions. In the Avacha active volcano rocks it is cementing diamond aggregate in association with cubic β-SiC, amorphous SiO_2 and tridymite, formed as a result of CVD processes during the course or shortly after the volcanic eruption (Kaminsky et al., 2016). Earlier we identified natural silicon Si^0 within the matrix of the carbonado-like polycrystalline diamond from the Avacha volcano, Kamchatka (Kaminsky et al., 2016). Here, we identified this phase as an open-framework allotrope of silicon S_{24}, which has been observed, to date, as a synthetic phase only (Kim et al., 2015), suggested to be a superconductor (Sung et al., 2018). According to Kim et al. (2015), low-pressure methods such as chemical vapor deposition (CVD) are the most efficient ways for its industrial production.

Amorphous masses comprise a significant part of the diamond aggregate matrix. In different parts of the sample they have various compositions: 'tilleyite—like' Ca-Si-C-O material (Fig. 4a), SiO_2 (Fig. 9) and amorphous carbon (Figs. 4b and 8), forming a transition to graphite. Silicides are heterogeneous in composition even within nanocrystals. Such heterogeneity is caused by very unstable, varying conditions during the course of the formation of the studied diamond aggregate.

Such features suggest the formation of the studied diamond aggregate, like the earlier studied Avacha aggregates (Kaminsky et al., 2016), at unstable near-atmospheric pressure conditions via gas phase condensation (chemical vapor deposition, CVD) during the course or shortly after the volcanic eruption, in a very reduced environment. The CVD mechanism of diamond formation is well known and is being widely used in the manufacturing of man-made diamonds (Dischler and Wild, 1998; Eaton-Magana and Shigley, 2016). In this mechanism, a material containing methane (CH_4) and hydrogen (H_2) is deposited from a gas onto a substrate. The following reactions take place:

$$2CH_4 + O_2 \rightarrow 4H_2 + 2CO;$$

307 $4H_2 + 2CO \rightarrow C$ (diamond) + H_2O.

308 The main requirements of diamond-producing CVD are: to deposit carbon onto the substrate and
309 simultaneously suppress the formation of graphitic sp^2-bonds. This is realized by establishing high
310 concentrations of non-diamond carbon etchants, such as atomic hydrogen (H_2) to the sourcing gas, and by
311 activating the gas either thermally or by plasma (http://www.cvd-diamond.com/geninfo_en.htm). The
312 typical growth temperatures are 700-900 °C, - similar to those established for the formation of the studied
313 aggregates. The most characteristic feature of CVD-grown diamonds is micro-twinning, observed in both
314 plasma (Shechtman et al., 1993; Dischler and Wild, 1998; Butler and Oleynik, 2008) and thermally
315 (Huang et al., 2011) activated products. Such a mechanism in diamond originates from the formation of a
316 hydrogen-terminated four-carbon atom cluster on a local {111} surface morphology, which also serves as
317 a nucleus for the next layer of growth. Subsequent growth proceeds by a reaction at the step edges with
318 one- and two-carbon-atom-containing species. The CVD mechanism of diamond formation with small
319 amounts of nitrogen added to the plasma assisted the growth environments, stimulating the dramatic
320 enhancement in polycrystalline diamond growth rates at temperatures in the range of 700–850 °C (Butler
321 and Oleynik, 2008).

322 No active volcanos exist now in the Valizhgen Peninsula, but Holocene (3-7 ka) volcanic cones are
323 known in the Aynyn River valley. They may be supposed as the sources of the studied diamond aggregate
324 sample.

325 The studied aggregates, both from Avacha and from Koryakia cannot be grown in the laboratory
326 because none of the identified mineral inclusions in diamond crystallites have been synthesized in CVD
327 diamonds, with the exception of tungsten carbide used as a substrate (Schwandler and Partes, 2011).
328 Moreover, some of newly found mineral species, such as an open-framework allotrope of silicon S_{24} was
329 synthesized only a few years ago (Kim et al., 2015), while the natural specimen Ayn-3 with S_{24} described
330 in this paper was found in the 1980s, when the CVD mechanism for the production of diamond only
331 started being developed.

332

6. Implications

The studied diamond aggregate from the Aynyn area in northern Kamchatka is similar, by its structure, composition and geological setting, to the earlier studied aggregates from the active Avacha volcano in southern Kamchatka (Kaminsky et al., 2016). In addition to earlier found unusual inclusions in diamond from the Avacha volcano, such as Mn–Ni–Si–Fe alloys (silicides), native Si^0, β-Mn, β-SiC, tungsten carbide W_2C, and boron carbide B_4C, which are uncommon for both carbonado and monocrystalline diamond, the Aynyn aggregate has in its composition tilleyite, three polymorphs of SiC (including cubic β-SiC), Fe-Ni-Mn-Cr silicides, graphite, calcite, native silicon and – for the first time in the natural environment – an open-framework allotrope of silicon Si_{24}, which has never been observed in nature before. Both the Avacha and Aynyn diamond aggregates are similar to carbonado, but have some differences. (1) They are related not to 'classic' diamond locations carbonado and of monocrystalline diamond within stable cratons, but to areas of active and Holocene volcanic belts. (2) Diamond crystallites in the studied aggregates are well-formed, sometimes idiomorphic, in contrast to usually irregular crystallites in carbonado. (3) Pores in the aggregates comprise 20-50 % of the volume, while in carbonado they do not exceed 20 vol.%. (4) Syngenetic mineral inclusions in the studied aggregates (Fe-Ni-Mn-Cr silicides, native β-Mn, tungsten carbide W_2C, and boron carbide B_4C) were never observed in carbonado and monocrystalline diamond. (5) Diamond crystallites are not sintered, like in carbonado, but cemented with amorphous SiO_2, tridymite, α- and β-SiC, native Si^0, calcite, tilleyite and graphite, which are not characteristic for carbonado. These features allow for the suggestion that diamond aggregates found in two areas within Kamchatka, in the Avacha volcano and in Koryakia, are a new diamond variety and may be called 'kamchatite'.

The most important feature of diamond crystallites is their micro- and nanotwinning, characteristic for a chemical vapor deposition (CVD) process. The synthetic analogs of all other, cementing minerals

(β-SiC, silicides and native silicon) formed by the CVD mechanism as well. This likely confirms the mechanism of CVD for the origin of 'kamchatite'.

Kamchatite extends the number of diamond varieties. In addition to monocrystalline diamond from kimberlites, lamproites and other magmatic rocks, formed at static high pressure-temperature conditions within the mantle; impact diamonds from meteoritic craters and meteorites, containing an admixture of lonsdaleite (yakutite) and formed as the result of solid-phase graphite transformation; diamonds from chromitites and metamorphic rocks, the genesis of which is still debatable; enigmatic carbonado; kamchatite represents diamond formed by gas phase condensation or chemical vapor deposition. Such variety of diamond, formed under various physic-chemical conditions, increases the potential sources of diamond and indicates the polygenetic character of diamond.

Acknowledgements

We thank Dr. A. Shiryaev for fruitful discussions of the described finds, Prof. A. Sobolev for his suggestion on the name 'kamchatite' for a new diamond variety, and Prof. D.Zedgenizov and an anonymous reviewer for their interesting, constructive reviews.

Appendix A. Supplementary data

Supplementary data to this article can be found online at …

References

382 Anand, M., Taylor, L.A., Nazarov, M.A., Shu, J., Mao, H.-K., Hemley, R.J. (2004) Space weathering on
383 airless planetary bodies: Clues from the lunar mineral hapkeite. Proceedings of the National
384 Academy of Sciences of the U.S.A. 101 (18), 6847-6851. DOI: 10.1073_pnas.0401565101.
385 Aronsson, B. (1958) An investigation of the Me_5Si_3 – MeSi region of the Mn-Fe-Si and related systems.
386 Acta Chemica Scandinavica 12(2), 308-313. DOI: 10.3891/acta.chem.scand.12-0308.
387 Bai, W., Robinson, P.T., Fang, Q., Yang, J., Yan, B., Zhang, Z., Hu, X., Zhou, M., Malpas, J. (2000) The
388 PGE and base-metal alloys in the podiform chromitites of the Luobusa ophiolite, southern Tibet.
389 Canadian Mineralogist 38(3), 585-598. DOI: 10.2113/gscanmin.38.3.585.
390 Bai, W., Shi, N., Fang, Q., Li, G., Xiong, M., Yang, J., Rong, H. (2006) Luobusaite: a new mineral. Acta
391 Geologica Sinica 80(5), 656–659.
392 Baikov, A.I., Anikin, L.P., Dunin-Barkovsky, R.L. (1995) Find of carbonado in volcanic rocks of
393 Kamchatka. Doklady AN SSSR 343(1), 72-74 (in Russian).
394 Ballhaus, C., Wirth, R., Fonseca, R.O.C., Blanchard, H., Pröll, W., Bragagni, A., Nagel, T., Schreiber, A.,
395 Dittrich, S., Thome, V., Hezel, D.C., Below, R., Cieszynski, H. (2017) Ultra-high pressure and
396 ultra-reduced minerals in ophiolites may form by lightning strikes. Geochemical Perspectives
397 Letters, 5, 42-46. Doi:10.7185/geochemlet.1744.
398 Bauer, J., Fiala, J., Hřichová, R. (1963) Natural α-Silicon carbide. American Mineralogist 48(5-6), 620-
399 634.
400 Beard, D., Drake, S.M. (2016) A melilite-bearing high-temperature calcic skarn, Camasunary Bay, Isle of
401 Skye. Scottish Journal of Geology 43, 57-67. DOI: 10.1144/sjg43010057.
402 Bińczyska, H., Dimitrijević, Z., Gajić, B., Szytuła, A. (1973) Atomic and magnetic structure of $Mn_{5-x}Fe_xSi_3$.
403 Physica Status Solidi (A) Applications and Materials Science 19(1), K13-K17.
404 DOI: 10.1002/pssa.2210190145.
405 Bird, J.M., Weathers, M.S. (1975) Josephinite: Specimens from the Earth's core? Earth and Planetary
406 Science Letters 28(1), 51-64. DOI: 10.1016/0012-821X(75)90073-4.

Butler, J.E., Oleynik, I. (2008) A mechanism for crystal twinning in the growth of diamond by chemical vapour deposition. Philosophical Transactions of the Royal Society A 366, 295–311. DOI: 10.1098/rsta.2007.2152.

Cabri, L.J., McDonald, A.M., Stanley, C.J., Rudashevsky, N.S., Poirier, G., Wilhelmij, H.R., Zhe, W., Rudashevsky, V.N. (2015) Palladosilicide, Pd_2Si, a new mineral from the Kapalagulu Intrusion, Western Tanzania and the Bushveld Complex, South Africa. Mineralogical Magazine 79, 295–307. DOI: 10.1180/minmag.2015.079.2.08.

Di Pierro, S., Gnos, E., Grobety, B. H., Armbruster, T., Bernasconi, S. M., Ulmer, P. (2003) Rock-forming moissanite (natural α-silicon carbide). American Mineralogist 88(11-12), 1817-1821.

Dischler, B., Wild, C. (1998) Low-pressure synthetic diamond. Manufacturing and applications. Springer Series in Materials Processing. Springer Verlag Berlin, Heidelberg.

Dobrzhinetskaya, L., Mukhin, P., Wang, Q., Wirth, R., O'Bannon, E., Zhao, W., Eppelbaum, L., Sokhonchuk, T. (2018) Moissanite (SiC) with metal-silicide and silicon inclusions from tuff of Israel: Raman spectroscopy and electron microscope studies. Lithos (in press). DOI: 10.1016/j.lithos.2017.04.001.

Eaton-Magana, S., Shigley, J.E. (2016) Observations on CVD grown synthetic diamonds: a review. Gems and Gemology 52(3), 222-245.

Essene, E.J., Fisher, D.C. (1986) Lightning strike fusion: extreme reduction and metal-silicate liquid immiscibility. Science 234(4773), 189–193. DOI: 10.1126/science.234.4773.189.

Fleishner, M. (1969) New mineral names. American Mineralogist 54(12), 1737.

Gevorkyan, V.Kh. (1969) The occurrence of natural ferrosilicon in the northern Azov region. Doklady Akademii Nauk SSSR 185, 416-418 (in Russian).

Gevorkyan, V.Kh., Litvin, A.L., Povarennykh, A.S. (1969) Occurrence of the new minerals fersilicite and ferdisilicate. Geologicheskii Zhurnal (Ukraine) 29(2), 62-71 (in Russian).

Golovko, A.V., Kaminsky, F.V. (2010) The shoshonite-absarokite-picrite Karashoho pipe, Uzbekistan: An unusual diamond deposit in atypical tectonic environment. Economic Geology 105(4), 825-840.

433 Golubkova, A., Schmidt, M.W., Connolly, J.A.D. (2016) Ultra-reducing conditions in average mantle
434 peridotites and in podiform chromitites: a thermodynamic model for moissanite (SiC) formation.
435 Contributions to Mineralogy and Petrology 171, 41. DOI 10.1007/s00410-016-1253-9.
436 Gorshkov, A.I., Seliverstov, V.A., Baikov, A.I., Anikin, L.P., Sivtsov, A.V., Dunin-Barkovsky, R.L.
437 (1995) Crystallochemistry and genesis of carbonado from the melanocratic basaltoids of the
438 Avacha volcano, Kamchatka Peninsula. Geology of Ore Deposits 37(1), 54-66 (in Russian).
439 Grice, J.D. (2005) The structure of spurrite, tilleyite and scawitte, and relations to other silicate-carbonate
440 minerals. Canadian Mineralogist 43, 1489-1500. DOI: 10.2113/gscanmin.43.5.1489.
441 Griffin, W.L., Gain, S.E.M., Adams, D.T., Huang, J.-X., Saunders, M., Toledo, V., Pearson, N.J.,
442 O'Reilly, S.Y. (2016) First terrestrial occurrence of tistarite (Ti2O3): Ultralow oxygen fugacity in
443 the upper mantle beneath Mt Carmel, Israel. Geology 44, 815-818. DOI: 10.1130/G37910.1.
444 Harker, R.I. (1959) The synthesis and stability of tilleyite, $Ca_5Si_2O_7(CO_3)_2$. American Journal of Science
445 257(9), 656-667. DOI: 10.2475/ajs.257.9.656.
446 He, D., Liu, Y., Gao, C., Chen, C., Hu, Z., Gao, S. (2017) SiC dominated ultrareduced mineral
447 assemblage in carbonatitic xenoliths from the Dalihu basalt, Inner Mongolia, China. American
448 Mineralogist 102, 312-320. DOI: 10.2138/am-2017-5721.
449 Hough, R.M., Gilmour, I., Pillinger, C.T., Arden, J.W., Gilkess, K.W.R., Yuan, J., Milledge, H.J.
450 (1995) Diamond and silicon carbide in impact melt rock from the Ries impact crater. Nature
451 378, 41–44. DOI: 10.1038/378041a0.
452 Hu, X.-F. (1999) Origin of diamonds in chromitites of the Luobusa ophiolite, southern Tibet, China.
453 M.Sc. Thesis, Dalhousie University, Halifax, Nova Scotia, Canada, 151 pp.
454 Huang, Y.-S., Luo, C.-P., Qiu, W.-Q., Liu, H.-W. (2011) Fivefold Twin Center in CVD Diamond Film.
455 Materials Science Forum 663-665, 1004-1007.
456 Kaminsky, F.V. (2007) Non-kimberlitic diamondiferous igneous rocks: 25 years after. In: Fareeduddin
457 and Rao, M.S. (Editors), Kimberlite and Related Rocks of India. Special Issue of Journal
458 Geological Society of India 69 (3), 557-575.

459 Kaminskiy, F.V., Bukin, V.I., Potapov, S.V., Arkus, N.G., Ivanova, V. G. (1969) Discoveries of silicon
460 carbide under natural conditions and their genetic importance. International Geology Review 11(5),
461 561-569. DOI: 10.1080/00206816909475090.
462 Kaminsky, F.V., Wirth, R., Anikin, L.P., Morales, L., Schreiber, A. (2016) Carbonado-like diamond from
463 the Avacha active volcano in Kamchatka, Russia. Lithos 265, 222-236. DOI:
464 10.1016/j.lithos.2016.02.021.
465 Kim, D.Y., Stefanoski, S., Kurakevych, O.O., Strobel, T.A. (2015) Synthesis of an open-framework
466 allotrope of silicon. Nature Materials 14, 169 – 173. DOI: 10.1038/nmat4140.
467 Kojima, T., Sakata, M., Nishida, I. (1990) Study on the formation of $Fe_{1-x}Mn_xSi_2$ fom the sintered FeSi -
468 Fe_2Si_5 eutectic alloy doped with manganese. Journal of the Less-Common Metals 162, 39-49.
469 Korzhinskii, M.A., Tkachenko, S.I., Bulgakov, R.F., Shmulovich, K.I. (1996) Condensate compositions
470 and native metals in sublimates of high-temperature gas streams of Kudrryavyi volcano, Iturup
471 island, Kuril islands. Geochemistry international 34(12), 1057-1064.
472 Kutyev, F.Sh., Kutyeva, G.V. (1975) Diamonds in basaltoids of Kamchatka. Doklady Akademii Nauk
473 SSSR 221(1), 183-186 (in Russian).
474 Landrum, G.A., Hoffmann, R., Evers, J., Boysen, H. (1998) The TiNiSi family of compounds: structure
475 and bonding. Inorganic Chemistry 37(22), 5754 – 5763. DOI**:** 10.1021/ic980223e.
476 Larsen, E.S., Dunham, K. (1933) Tilleyite, a new mineral from the contact zone at Crestmore, California.
477 American Mineralogist 18(11), 469-473.
478 Leung, I., Guo, W., Friedman, I., Gleason, J. (1990) Natural occurrence of silicon carbide in a
479 diamondiferous kimberlite from Fuxian. Nature 346, 352-354.
480 Li, G., Fang, Q., Shi, N., Bai, W., Yang, J., Xiong, M., Ma, Z., Rong, H. (2009) Zangboite, $TiFeSi_2$, a
481 new mineral species from Luobusha, Tibet, China, and its crystal structure. Canadian Mineralogist
482 47(5), 1265-1274. DOI: 10.3749/canmin.47.5.1265.

Li, G., Bai, W., Shi, N., Fang, Q., Xiong, M., Yang, J., Ma, Z., Rong, H. (2012) Linzhiite, $FeSi_2$, a redefined and revalidated new mineral species from Luobusha, Tibet, China. European Journal of Mineralogy 24(6), 1047-1052. DOI: 10.1127/0935-1221/2012/0024-2237.

Marshintsev, V.K. (1990) Natural silicon carbide in kimberlitic rocks of Yakutiya. Mineralogicheskii Zhurnal 12(3), l7- 26 (in Russian).

Marshintsev, V.K., Tshelchkova, S.G., Zolnikov, G.V., Voskresenskaya, V.B. (1967) New data on moissanite from kimberlites of Yakutia. Russian Geology and Geophysics, no. 12, 22-31 (in Russian).

Mitchell, R. H. (1997) Carbonate-carbonate immiscibility, neighborite and potassium iron sulphide in Oldoinyo Lengai natrocarbonatite. Mineralogical Magazine, 61(6), 779-789.

Nakamura-Messenger, K., Keller, L.P., Clemett, S.J., Messenger, S., Jones, J.H., Palma, R.L., Pepin, R.O., Klöc , W., Zolensky, M.E., Tatsuoka, H. (2010) Brownleeite: A new manganese silicide mineral in an interplanetary dust particle. American Mineralogist 95(2-3), 221-228. DOI: 10.2138/am.2010.3263.

Nazarov, M.A., Demidova, S.I., Anosova, M.O., Kostitsyn, Y.A., Ntaflos, T., Brandstaetter, F. (2012) Native silicon and iron silicides in the Dhofar 280 lunar meteorite. Petrology 20(6), 506-519.

Nicolet, M.A., Lau, S.S. (1983) Formation and characterization of transition-metal silicides. VLSI Electronics Microstructure Science 6, 329-464. DOI: 10.1016/B978-0-12-234106-9.50011-8.

Nockolds, S.R., Vincent, H.G.C. (1947) On tilleyite and its associated minerals from Carlingford, Ireland. Mineralogical Magazine 28(198), 151-158.

Novgorodova, M.I., Boronikhin, V.A., Generalov, M.E., Kramer, K. (1989) On native silicon in association with native gold and other metals. Doklady Akademii Nauk SSSR 309(5), 1182-1185 (in Russian).

Novoselova, L.N., Bagdasarov, E.A. (1979) New data on iron silicides. Zapiski VMO 106(3), 326-333 (in Russian).

508 Osipenko, A.B., Sidorov, E., Kostoyanov, A.I., Tolstykh, N.D. (2002) Chromitites of ultramafic
509 complexes of the Valizhgen Peninsula, Koryak Highland. Geology of Ore Deposits 44(1), 69-83.
510 Pankov, V.Yu., Spetsius, Z.V. (1989) Inclusions of iron silicides and native silicon in moissanite from
511 the Sytykan kimberlite pipe. Doklady Akademii Nauk SSSR 305(3), 704–708 (in Russian).
512 Regis, A.I., Sand, L.B. (1958) Natural cubic (β) silicon carbide. Geological Society of America Bulletin
513 69(12), 1633-1643.
514 Rietmeijer, F.J.M., Nakamura, T., Tsuchiyama, A., Uesugi, K., Nakano, T., Leroux, H. (2008) Origin and
515 formation of iron silicide phases in the aerogel of the Stardust mission. Meteoritics and Planetary
516 Science 43(1/2), 121–134.
517 Rubenach, M.J., Cuff, C. (1985) The occurrence of coarse-grained massive tilleyite in the Redcap Creek
518 magmatic skarn, North Queensland. Mineralogical Magazine 49(350), 71-75.
519 DOI: 10.1180/minmag.1985.049.350.09.
520 Sazonov, A.M., Zvyagina, E.A., Leontyev, S.L., Vulf, M.V., Poleva, T.V., Checkushin, V.S., Oleynikova,
521 N.V. (2008) Associations of micro- and nanosize isolations of the precious metals complex in ores.
522 Journal of Siberian Federal University. Engineering and Technologies 1(1), 17-32 (in Russian).
523 Schwander, M., Partes, K. (2011) A review of diamond synthesis by CVD processes. Diamond and
524 Related Materials 20(9), 1287-1301. DOI: 10.1016/j.diamond.2011.08.005.
525 Seliverstov, V.A. (2009) Thermobarophyllic mineral paragenesrs of diamondiferous alkaline ultramafic
526 volcanic complex in Eastern Kamchatka. Vestnik KRAUNZ Earth Sciences № 1(13), 10-30 (in
527 Russian).
528 Shechtman, D., Hutchison, J.L., Robins, L.H., Farabaugh, E.N., Feldman, A. (1993) Growth defects in
529 diamond films. Journal of Materials Research 8(3), 473-479.
530 Shi, N., Bai, W., Li, G., Xiong, M., Yang, J., Ma, Z., Rong, H. (2012) Naquite, FeSi, a new mineral
531 species from Luobusha, Tibet, Western China. Acta Geologica Sinica 86(3), 533–538.

Shilo, N.A., Kaminskiy, F.V., Lavrova, L.D., Dolmatov, B.K., Pleshakov, A.P., Tkachenko, L.A., Shepeleva, K.A. (1979) First diamond find in ultrabasic rocks of Kamchatka. Doklady, Earth Science Sections 248, 176-179.

Shiryaev, A.A., Gaillard, F. (2014) Local redox buffering by carbon at low pressures and the formation of moissanite – natural SiC. European Journal of Mineralogy 26, 53–59. DOI: 10.1127/0935-1221/2013/0025-2339.

Shiryaev, A.A., Griffin, W.L., Stoyanov, E. (2011) Moissanite (SiC) from kimberlites: Polytypes, trace elements, inclusions and speculations on origin. Lithos 122(3-4), 152-164. DOI: 10.1016/j.lithos.2010.12.011.

Spicuzza, M.J., Valley, J.W., Fournelle, J., Huberty, J.M., Treiman, A. (2011) Native silicon and Fe-silicides from the Apollo 16 lunar regolith: extreme reduction, metal-silicate immiscibility, and shock melting. 42nd Lunar and Planetary Science Conference Abstract #2231.

Sung, H.-J., Han, W.H., Lee, I.-H., Chang, K.J. (2018) A new superconducting open-framework allotrope of silicon at ambient pressure. Physical Review Letters 120, 157001. DOI: 10.1103/PhysRevLett.120.157001.

Tatarintsev, V.I., Tsymbal, S.N., Sandomirskaya, S.M., Egorova, L.N., Vashtchenko, A.N., Khnyazkov, A.P. (1990) Iron-bearing manganese silicides from the Priazovye (USSR). Mineralogicheskii Zhurnal 12(6), 35-43 (in Russian).

Tishchenko, A.I., Kasatkin, A.V., Shkoda, R. (2016) Silicides (naquite, linzhiite, luobusaite and zangboite) in Sarmatian limestones of Crimea. Noviye Danniye o Mineralakh (New Data on Minerals) 51, 30-37 (in Russian).

Trumbull, R. B., Yang, J. S., Robinson, P. T., Di Pierro, S., Vennemann, T., Wiedenbeck, M. (2009) The carbon isotope composition of natural SiC (moissanite) from the Earth's mantle: New discoveries from ophiolites. Lithos 113, 612-620. DOI: 10.1016/j.lithos.2009.06.033.

556 Wirth, R. (2004) Focused ion beam (FIB): A novel technology for advanced application of micro- and
557 nanoanalysis in geosciences and applied mineralogy. European Journal of Mineralogy 16(6), 863-
558 877. DOI: 10.1127/0935-1221/2004/0016-0863.
559 Wirth, R. (2009) Focused Ion Beam (FIB) combined with SEM and TEM: Advanced analytical tools for
560 studies of chemical composition, microstructure and crystal structure in geomaterials on a
561 nanometre scale. Chemical Geology 261, 217-229. DOI: 10.1016/j.chemgeo.2008.05.019**.**
562 Yang, J., Meng, F., Xu, X., Robinson, P. T., Dilek, Y., Makeyev, A. B., Wirth, R., Wiedenbeck, M.,
563 Griffin, W. L., Cliff, J. (2015) Diamonds, native elements and metal alloys from chromitites of the
564 Ray-Iz ophiolite of the Polar Urals. Gondwana Research 27, 459–485. DOI:
565 10.1016/j.gr.2014.07.004.
566 Zhang, R. Y., Yang, J.-S., Ernst, W.G., Jahn, B.-M., Iizuka, Y., Guo, G.-L. (2016) Discovery of in situ
567 super-reducing, ultrahigh-pressure phases in the Luobusa ophiolitic chromitites, Tibet: New
568 insights into the deep upper mantle and mantle transition zone. American Mineralogist 101, 1285-
569 1294. DOI: 10.2138/am-2016-5436.
570
571
572 **Table title**
573
574 **Table 1**. The chemical compositions of Fe-Ni-Mn silicide grains (at.%)
575
576
577 **Captions to Figures**
578
579 **Fig. 1**. Scheme of the finds of carbonado-like diamond aggregate grains within the Valizhgen Peninsula,
580 northern Kamchatka, Russia, shown in stars. Blue – ultramafic massifs.
581

582 **Fig. 2**. Secondary electron image (SEI) of microcrystalline diamond aggregate from the Valizhgen
583 Peninsula, Koryakia, Kamchatka. Diamond crystallites (dark) cemented by nanocrystalline-amorphous
584 aggregate (white). Scale bar is 20 μm.
585
586 **Fig. 3**. Structure of diamond crystallites. a – Intense twinning and dislocations in foil #4975. b – High
587 dislocation density in foil #4976. HAADF overview images.
588
589 **Fig. 4**. Matrix of the diamond aggregate. a – Tilleyitic amorphous matrix with embedded nanograins of
590 SiC and Fe-Ni-Mn silicide. TEM bright-field image. Foil #4975. b – Amorphous tilleyitic-graphitic mass
591 cementing diamond crystallites. Thin graphite-containing layers are located between diamond and the
592 tilleyitic amorphous material. Diamond shows local very high dislocation density areas and intensive
593 twinning. TEM bright-field image. Foil #4976.
594
595 **Fig. 5**. Hexagonal crystal of Fe-Ni-Mn silicide between diamond grains. a – General view. TEM bright-
596 field image. Foil # 4976. b - Indexed diffraction pattern (FFT) of Fe-Ni-Mn silicide based on hexagonal
597 crystal structure.
598
599 **Fig. 6**. Chemical composition of the Fe-Ni-Mn-Cr silicides in diamond aggregate. a – General
600 composition. b – Composition of major cations. Group 1 (red squares) – $(Fe,Ni,Mn,Cr)_5Si_3$ hexagonal;
601 Group 2 (blue circles) - (Fe,Ni,Mn,Cr)Si cubic; Group 3 (green stars) - $(Fe,Ni,Mn,Cr)Si_2$. Comments in
602 the text.
603
604 **Fig. 7**. Open-framework allotrope of silicon Si_{24} from foil #5312. a - Mosaic grain composed of
605 nanocrystals of Si_{24}. Bright-field image. b - HAADF image of the mosaic crystal of Si_{24} showing the
606 individual nanocrystals. The inset image in the upper-right corner displays a higher magnification. Some
607 of the nanocrystals show nano-twin lamellae. c - High-resolution lattice fringe image of an individual

nanocrystal of Si_{24} from the mosaic crystal. Indexed diffraction pattern is inserted in the upper right corner. d - TEM dark-field image using the (141) reflection in diffraction pattern. The brighter patches in the mosaic crystal are individual nanocrystals of Si_{24} with a perfect zone axis orientation with respect to the electron beam. The alternating bright and dark contrasts at the crystal interfaces are thickness fringes due to an inclined interface.

Fig. 8. High-resolution lattice fringe image of graphite flake associated with amorphous carbon. The inserted diffraction pattern shows the (0002) reflections of graphite. The smeared-out appearance of the diffraction spots displays the distortion of the basal planes in graphite. Foil #4976.

Fig. 9. TEM bright-field image of porous calcite together with amorphous SiO_2 and carbon plus graphite. Foil #4976.

Supplementary data

Supplementary Table 1. Structural data of tilleyite

Supplementary Table 2. Structural data on hexagonal silicon carbides

Supplementary Table 3. Structural data of Fe-Ni-Mn-Cr silicides

Supplementary Table 4. Structural data of native silicon

Supplementary Fig. 1. Structure and composition of tilleyite. a - High-resolution lattice fringe image of grain HREM02 from foil #4975. The inset shows the indexed diffraction pattern according to tilleyite.

The observed *d*-spacings are presented in Supplementary Table 1. b and c – EDX spectra of crystalline (b) and amorphous (c) tilleyite, showing their similar chemical compositions. In these and other EDX spectra, the Cu–Kα X-ray intensity is due to the copper grid on which the sample rests, and the Ga X-ray intensity represents gallium implanted during the FIB sputtering.

Supplementary Fig. 2. High-resolution lattice fringe image of SiC indexed based on a cubic structure. Indexed diffraction pattern in the upper right corner. Foil #5317C.

Supplementary Fig. 3. Fe-Ni-Mn-Cr silicide in foil #4975 with variable chemical composition. a - TEM bright-field image. Numbers 3 and 4 indicate the locations of the analyses given in Supplementary Figs. 3b and 3c. b and c – EDX spectra collected at locations 3 and 4, respectively. While Fe peak intensities are almost similar in both spectra, the Si peak is significantly more intense and Mn and Ni peaks are significantly less intense in spectrum location 4 (spectrum "c"), while the Ti peak occurs only in spectrum location 3 (spectrum "b"); this reflects the variable chemical compositions observed in locations 3 and 4 (see Table 1).

Table 1. The chemical compositions of Fe-Ni-Mn silicide grains (at.%)

Foil #	Grain	Si	Ti	Fe	Mn	Ni	Cr	Total	(Fe+Mn+Ni+Cr / (Si+Ti)	Group
4975	3*	46.52	2.87	19.76	22.17	7.69	0.99	100.00	1.025	2
	4*	64.13	-	20.2	11.80	3.64	0.23	100.00	0.559	3
	HREM04 cubic	50.11	-	15.86	7.17	26.71	0.15	100.00	0.996	2
4976	HREM02 hexagonal	34.63	-	23.68	19.52	20.37	1.80	100.00	1.888	1
	1	63.87	0.04	5.56	15.94	14.01	0.58	100.00	0.565	3
	2	50.64	-	18.31	15.08	15.17	0.80	100.00	0.975	2
	3	49.03	0.49	5.11	24.22	19.13	2.02	100.00	1.019	2
	4	47.97	-	3.45	25.04	22.72	0.82	100.00	1.085	2
	5	45.19	-	16.56	20.71	17.54	-	100.00	1.213	
	6	39.78	-	24.81	20.29	14.66	0.46	100.00	1.514	
	7	34.19	-	25.95	22.16	16.74	0.96	100.00	1.925	1
	8	34.5	-	26.2	22.4	16.9	-	100.0	1.899	1
	9	51.0	-	18.4	15.2	15.4	-	100.0	0.961	2
5312	11	66.38	0.05	15.82	11.8	5.33	0.62	100.00	0.505	3
	12	66.01	-	16.52	12.52	4.72	0.23	100.00	0.511	3
5316B	21	62.32	-	9.73	26.98	0.65	0.32	100.00	0.605	3
5317C	31	60.85	-	19.76	11.23	8.11	0.05	100.00	0.643	
	32	60.60	-	23.03	8.84	7.53	-	100.00	0.650	

Note: *) Analyses #4975(3) and #4975(4) are from the same crystal (see Fig. 7a).

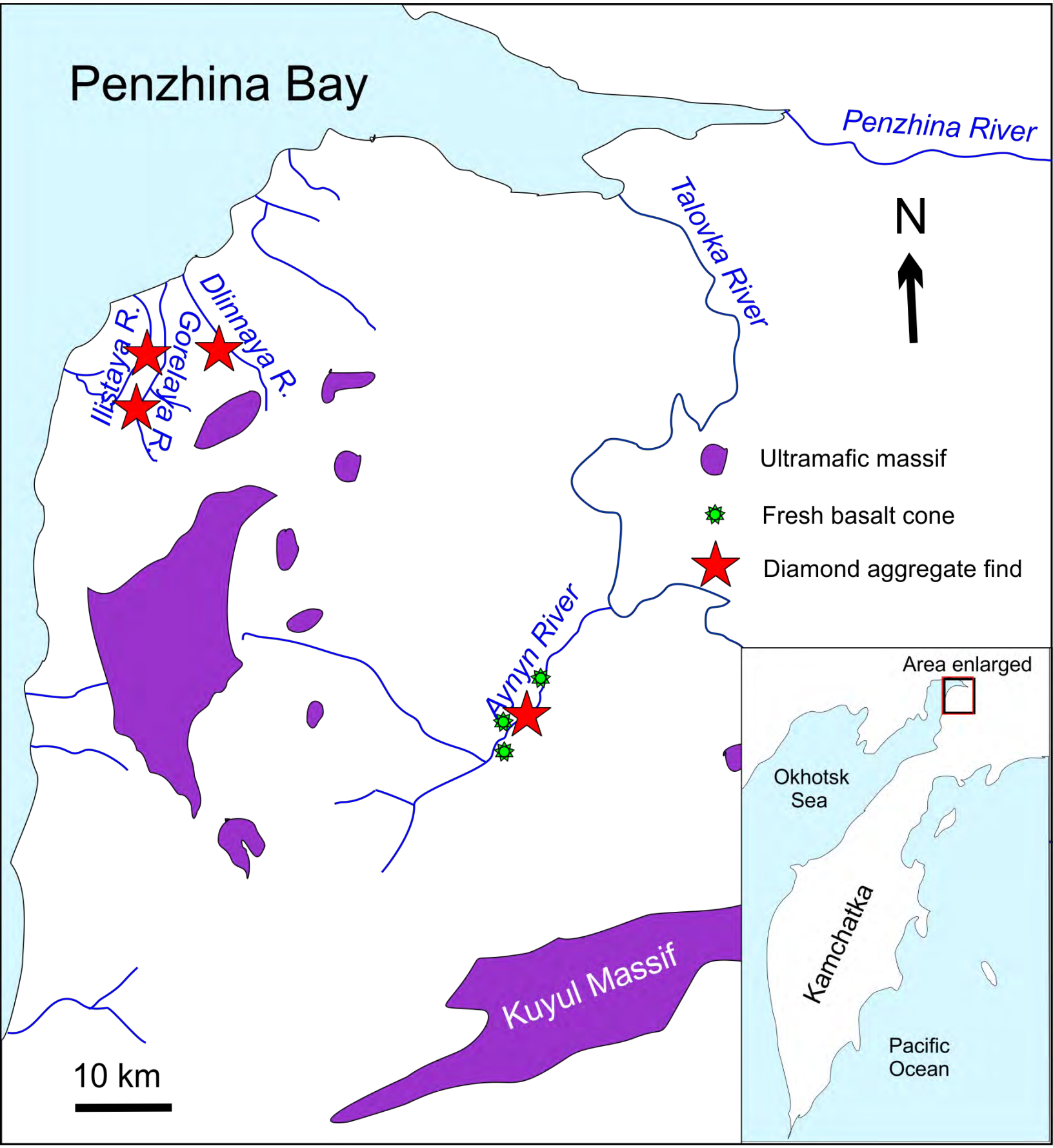
Penzhina Bay
Penzhina River
Talovka River
N
Ilistaya R.
Gorelaya R.
Dlinnaya R.
Ultramafic massif
Fresh basalt cone
Diamond aggregate find
Aynyn River
Area enlarged
Okhotsk Sea
Kamchatka
Pacific Ocean
Kuyul Massif
10 km

Figure 1

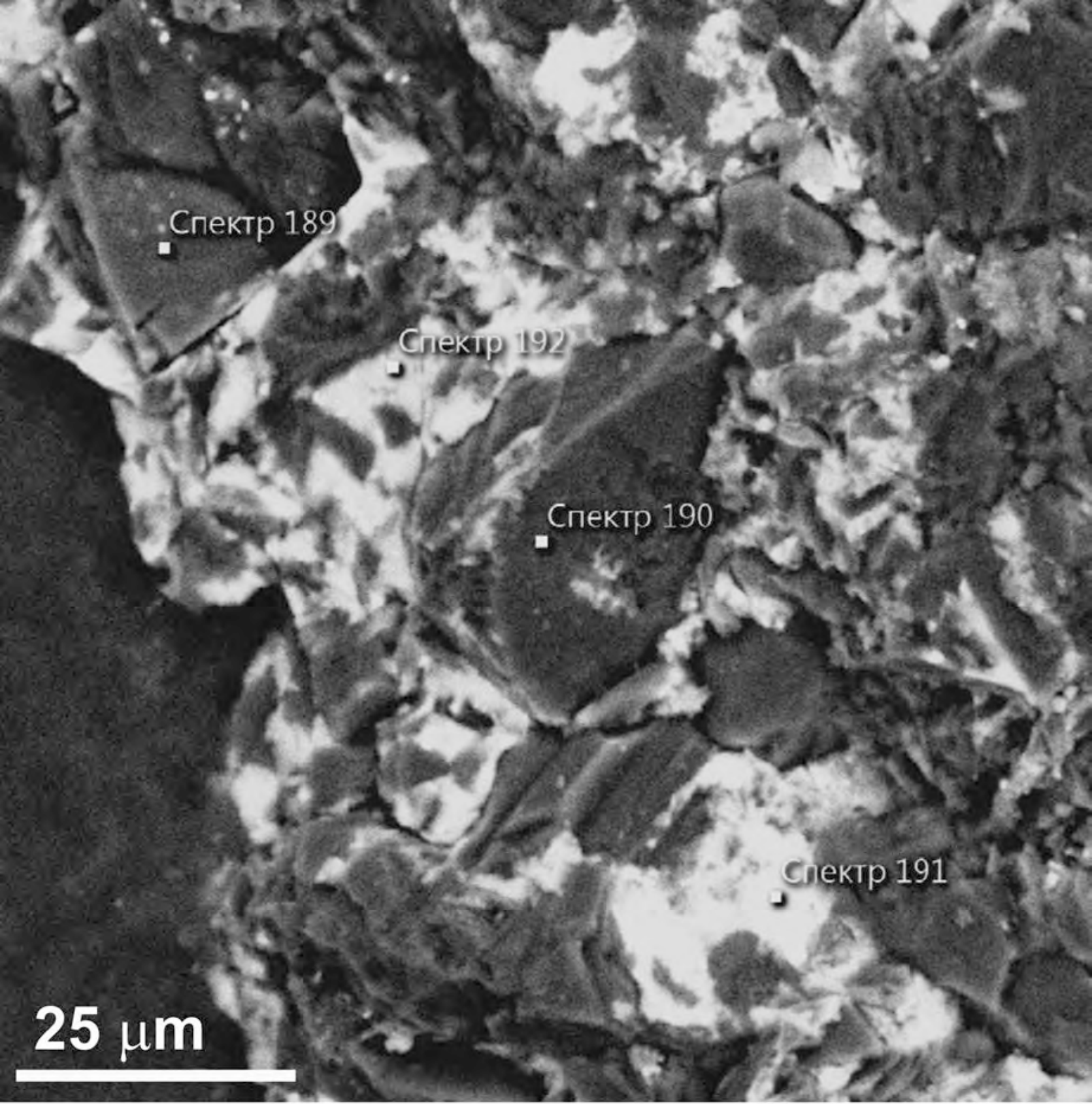

Figure 2

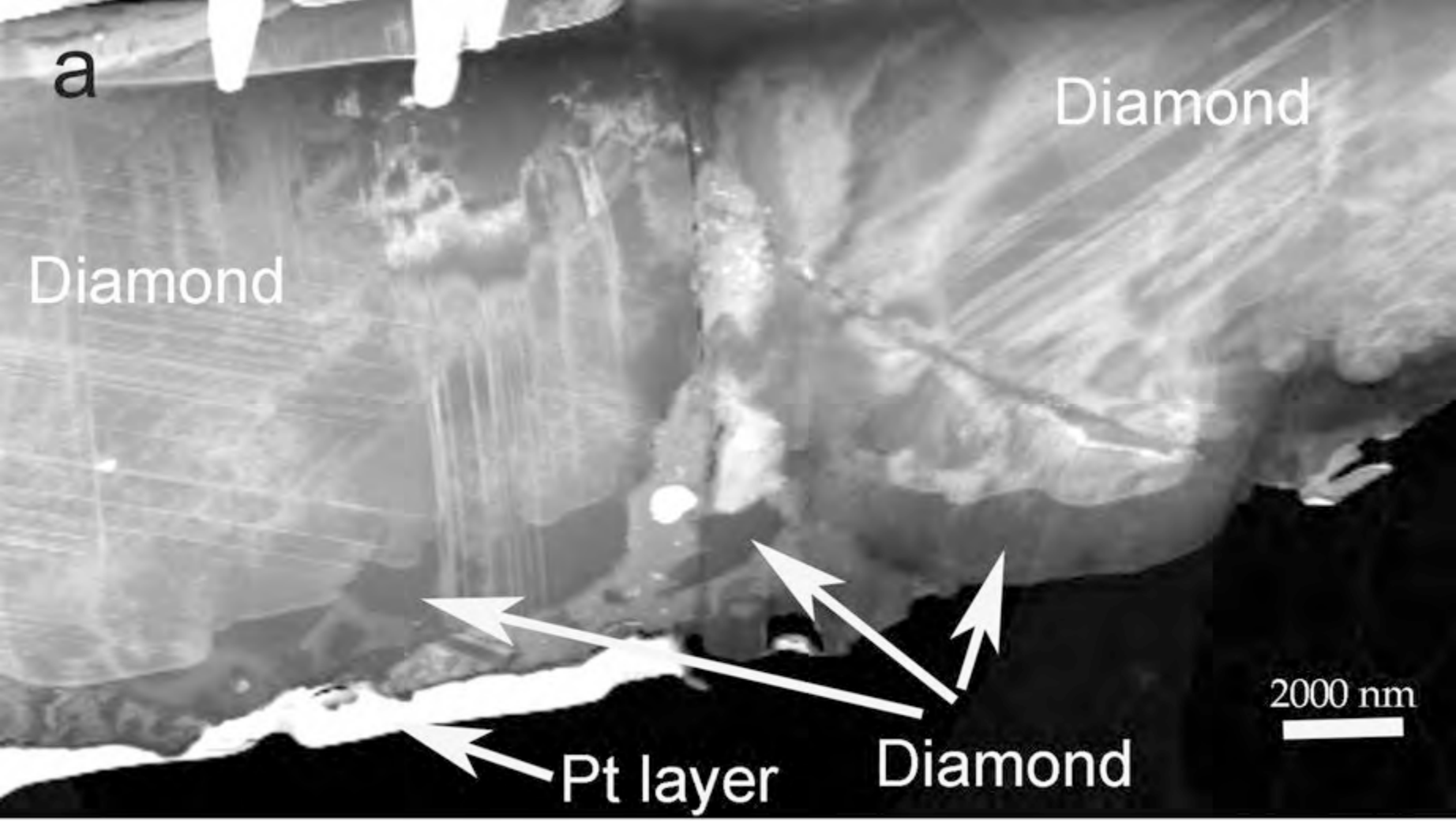

Figure 3a

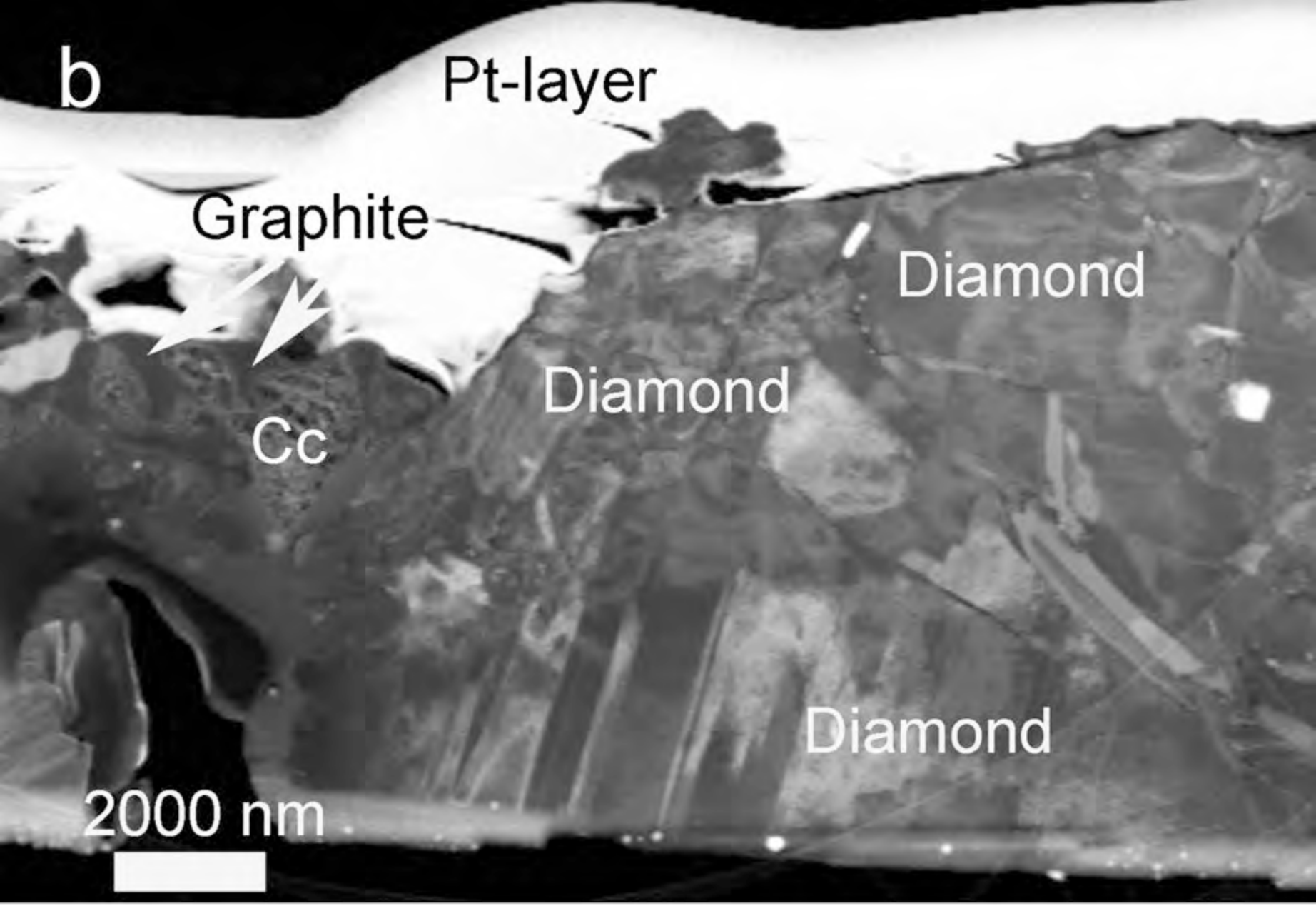

Figure 3b

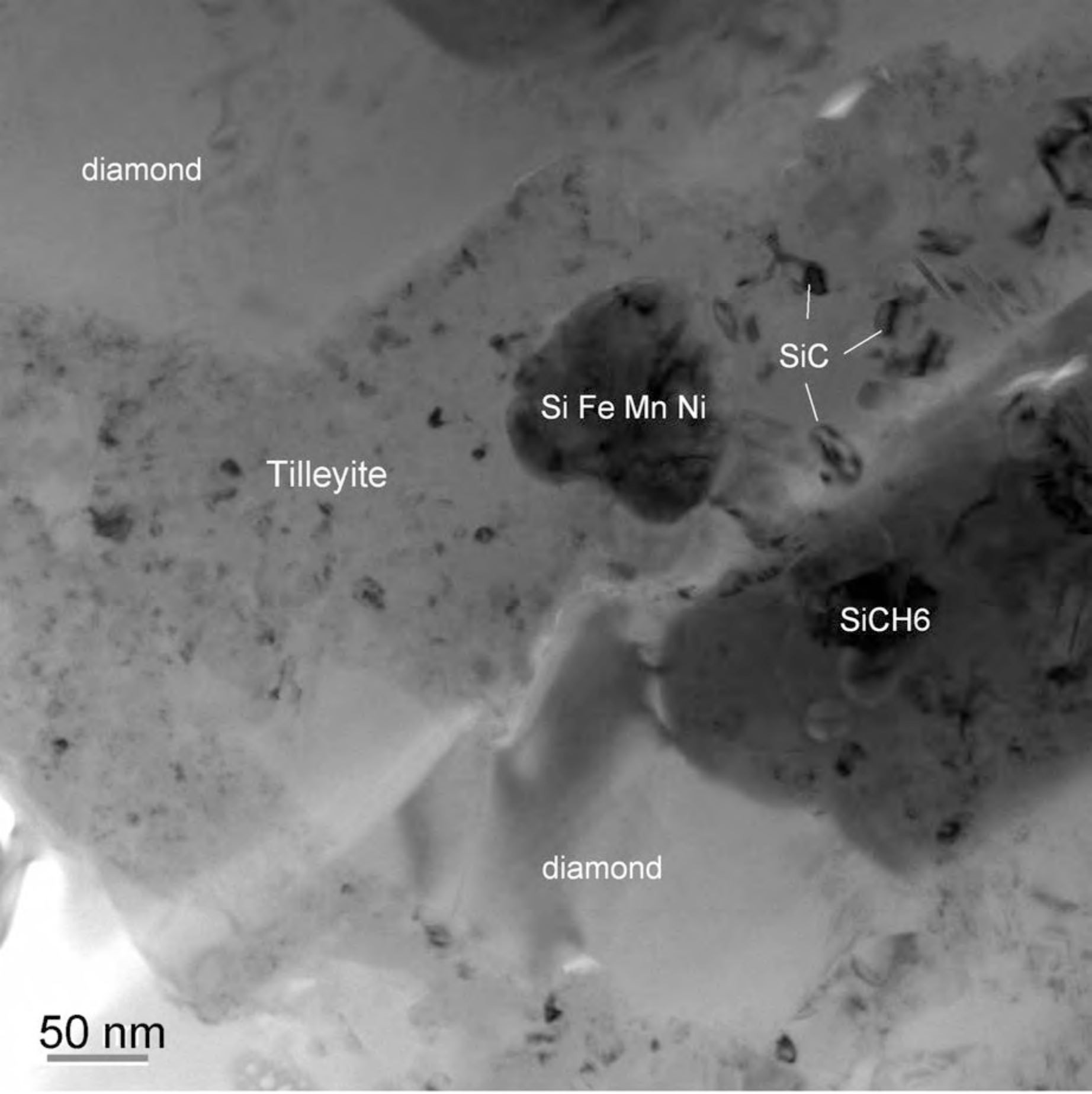

Figure 4a

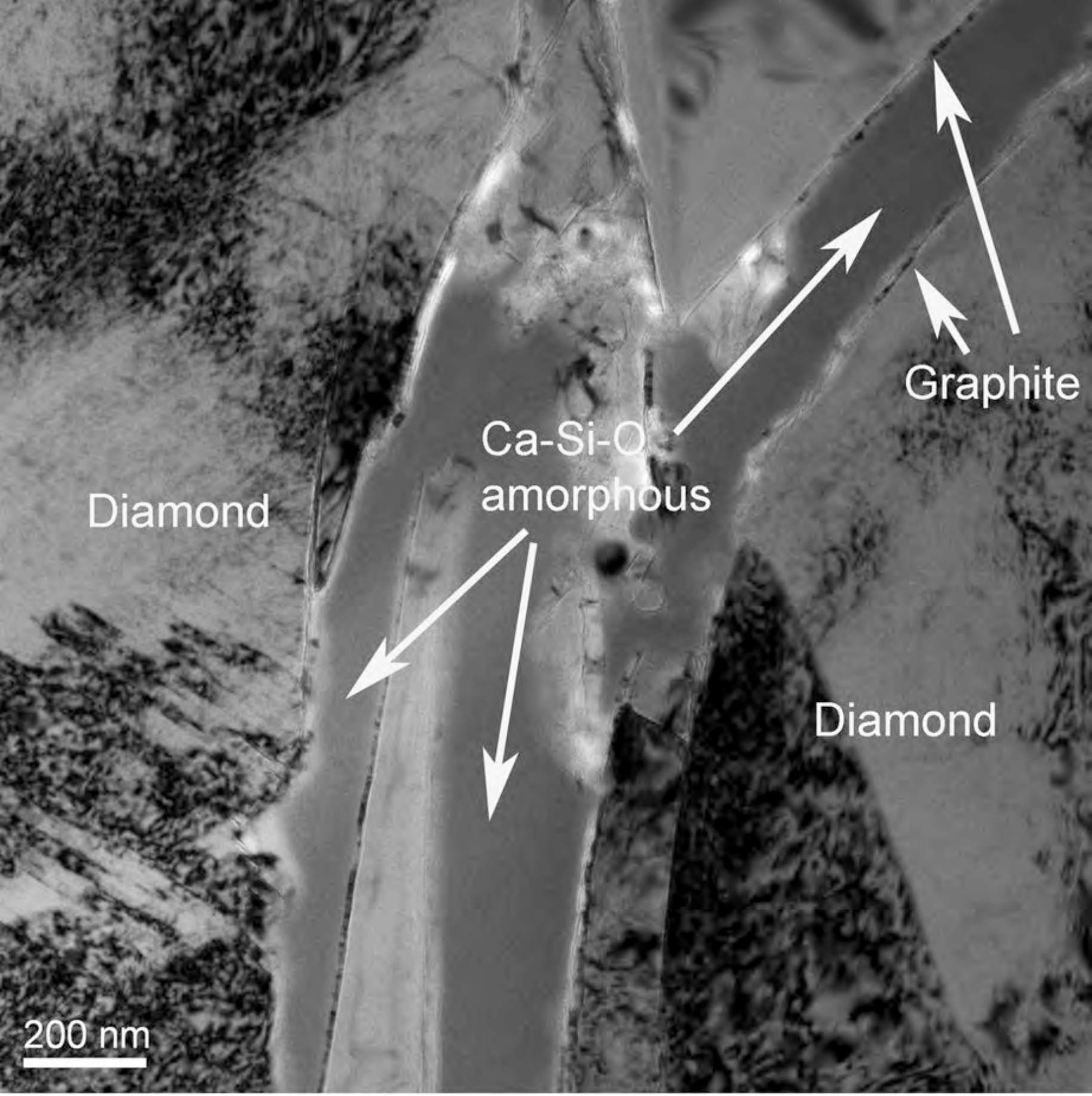

Figure 4b

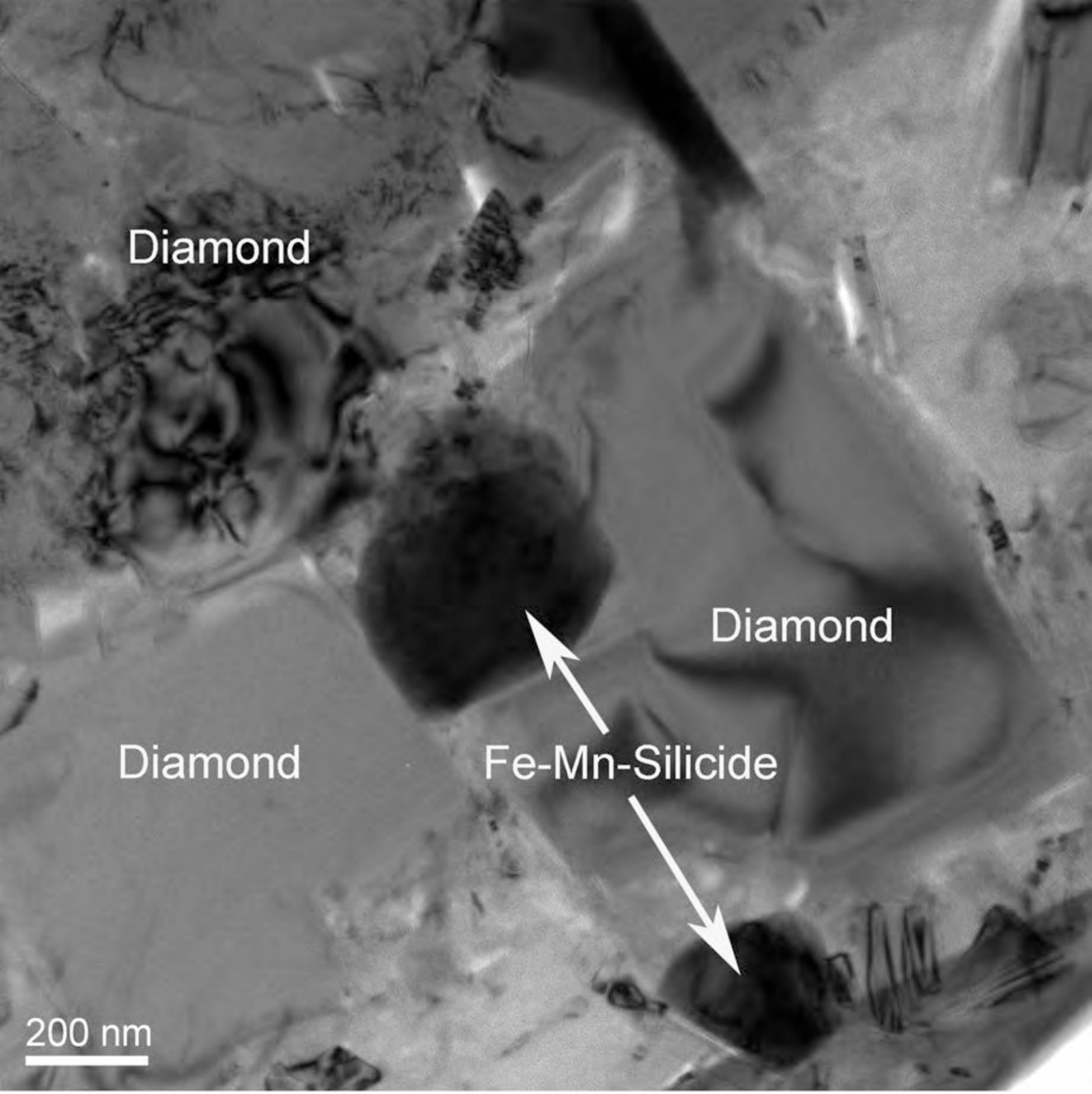

Figure 5a

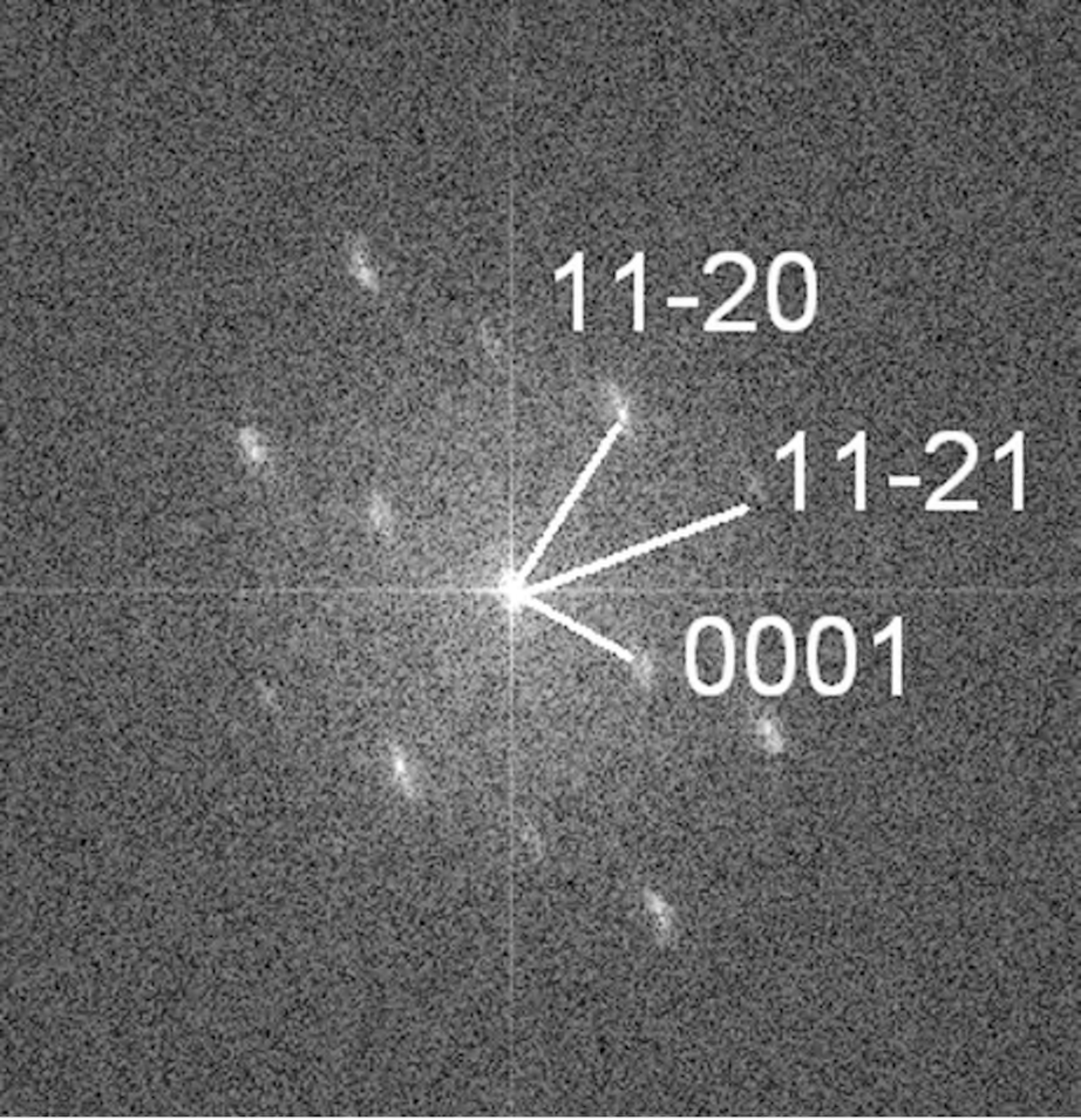

Figure 5b

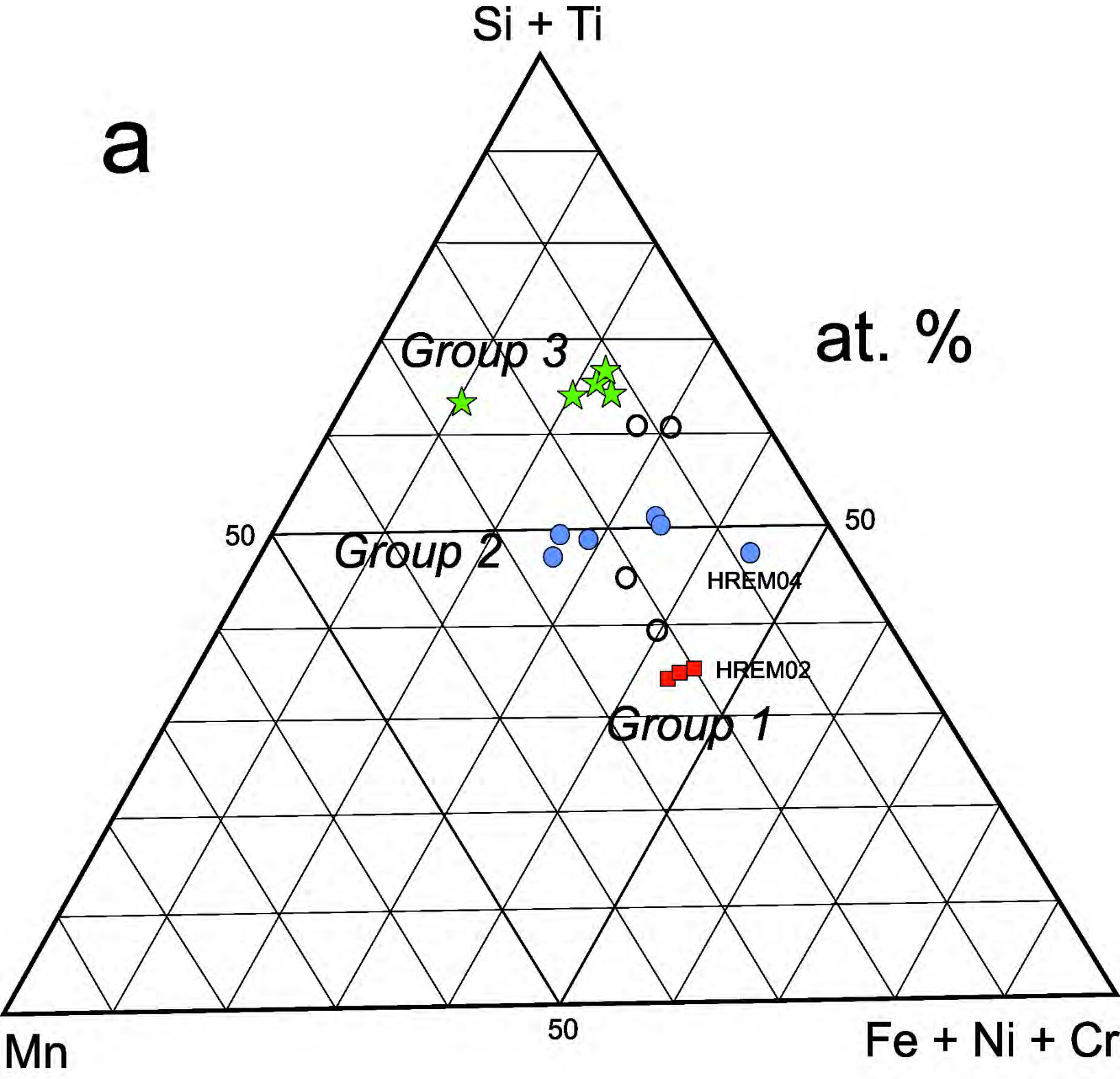
a
Si + Ti
at. %
Group 3
Group 2
Group 1
HREM04
HREM02
50
50
50
Mn
Fe + Ni + Cr

Figure 6a

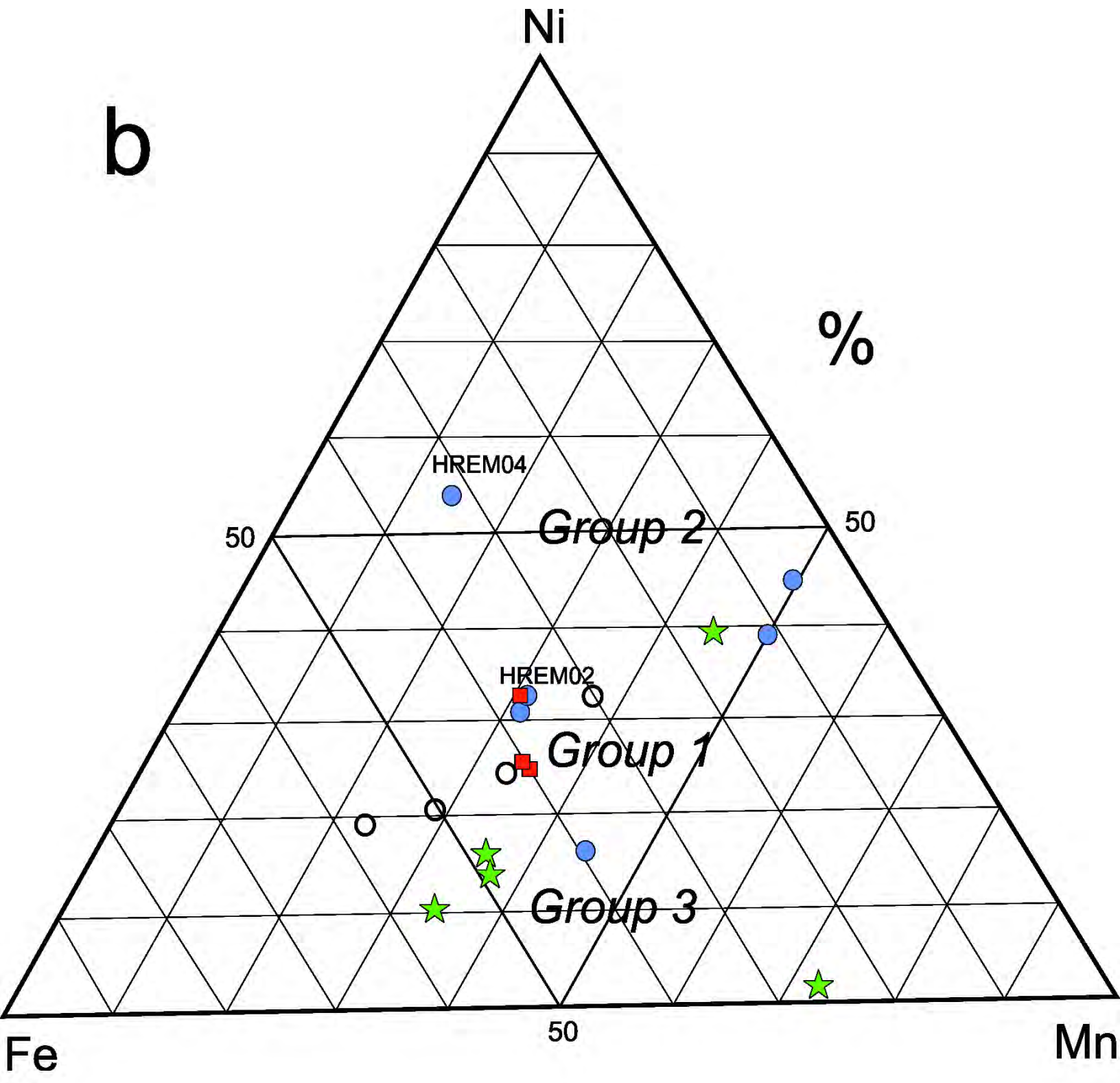

Figure 6b

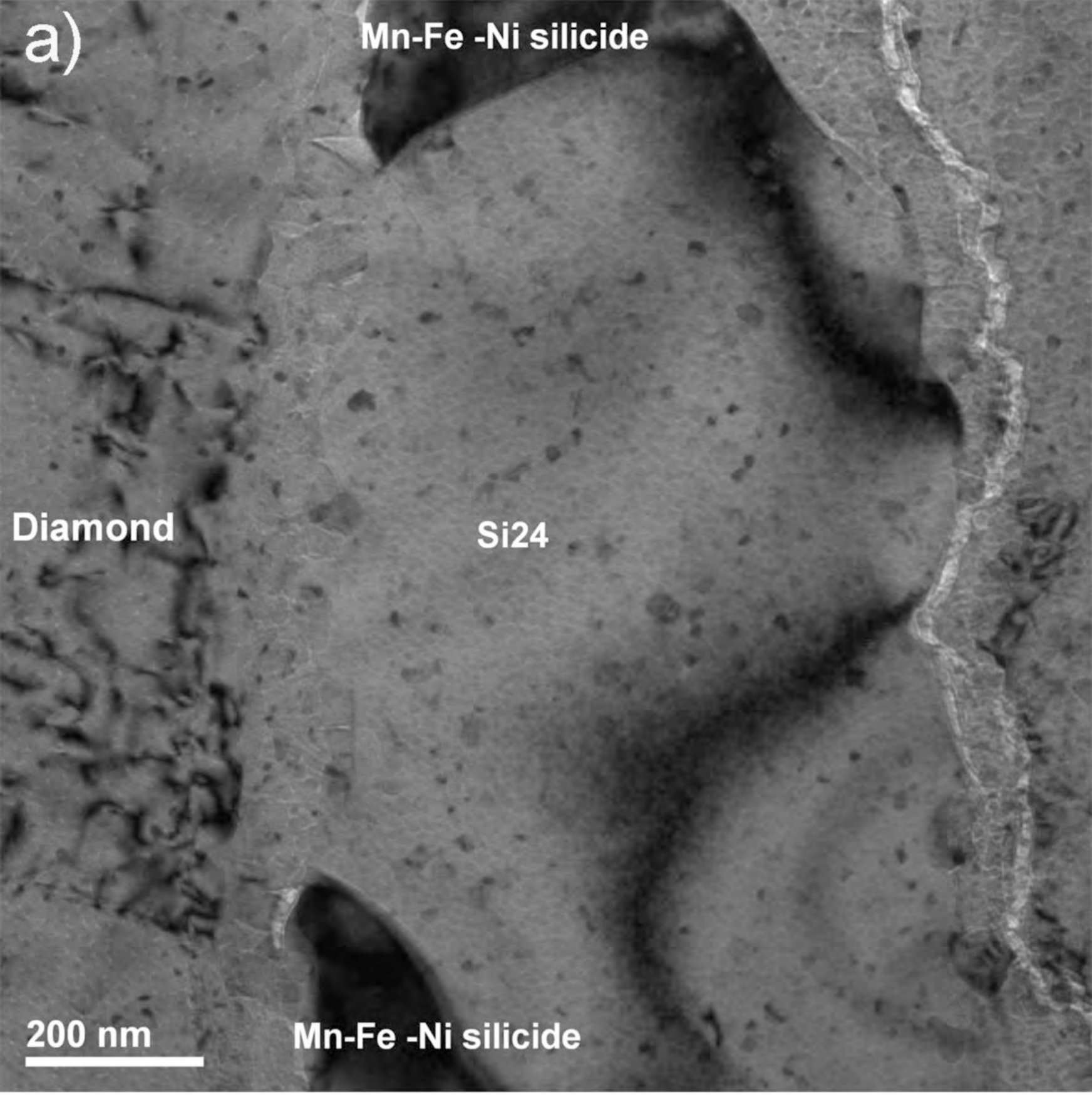

Figure 7a

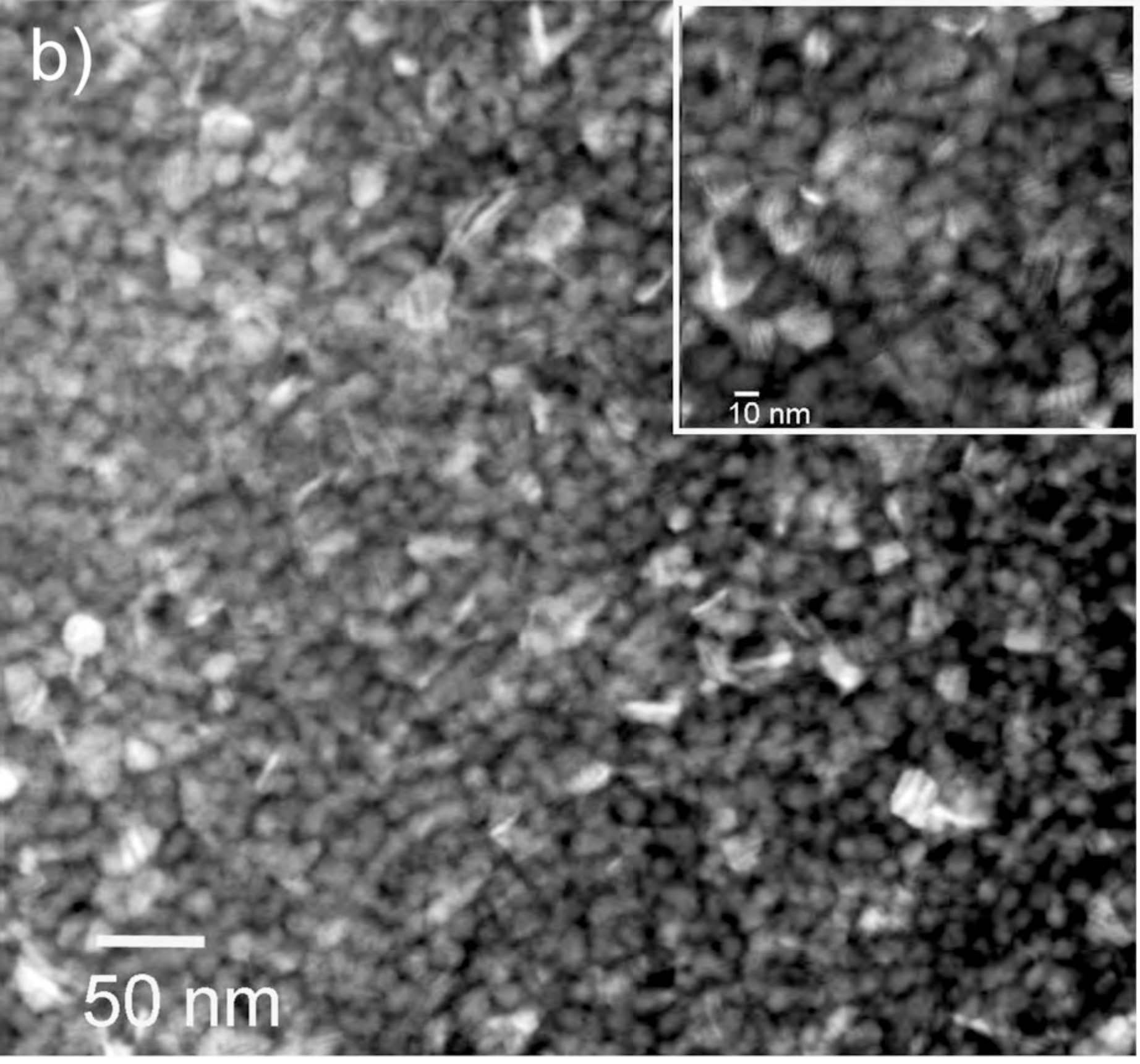

Figure 7b

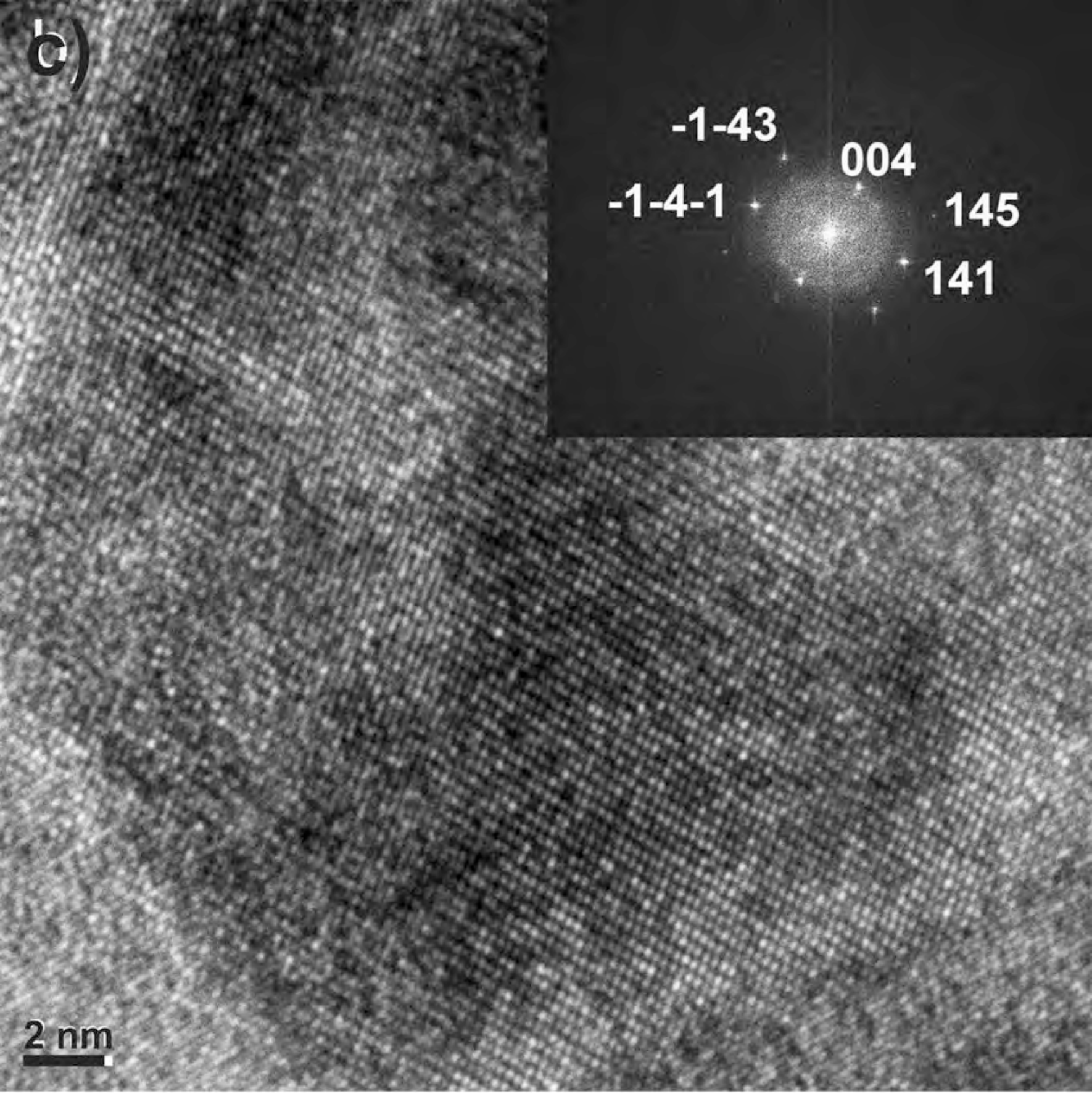

Figure 7c

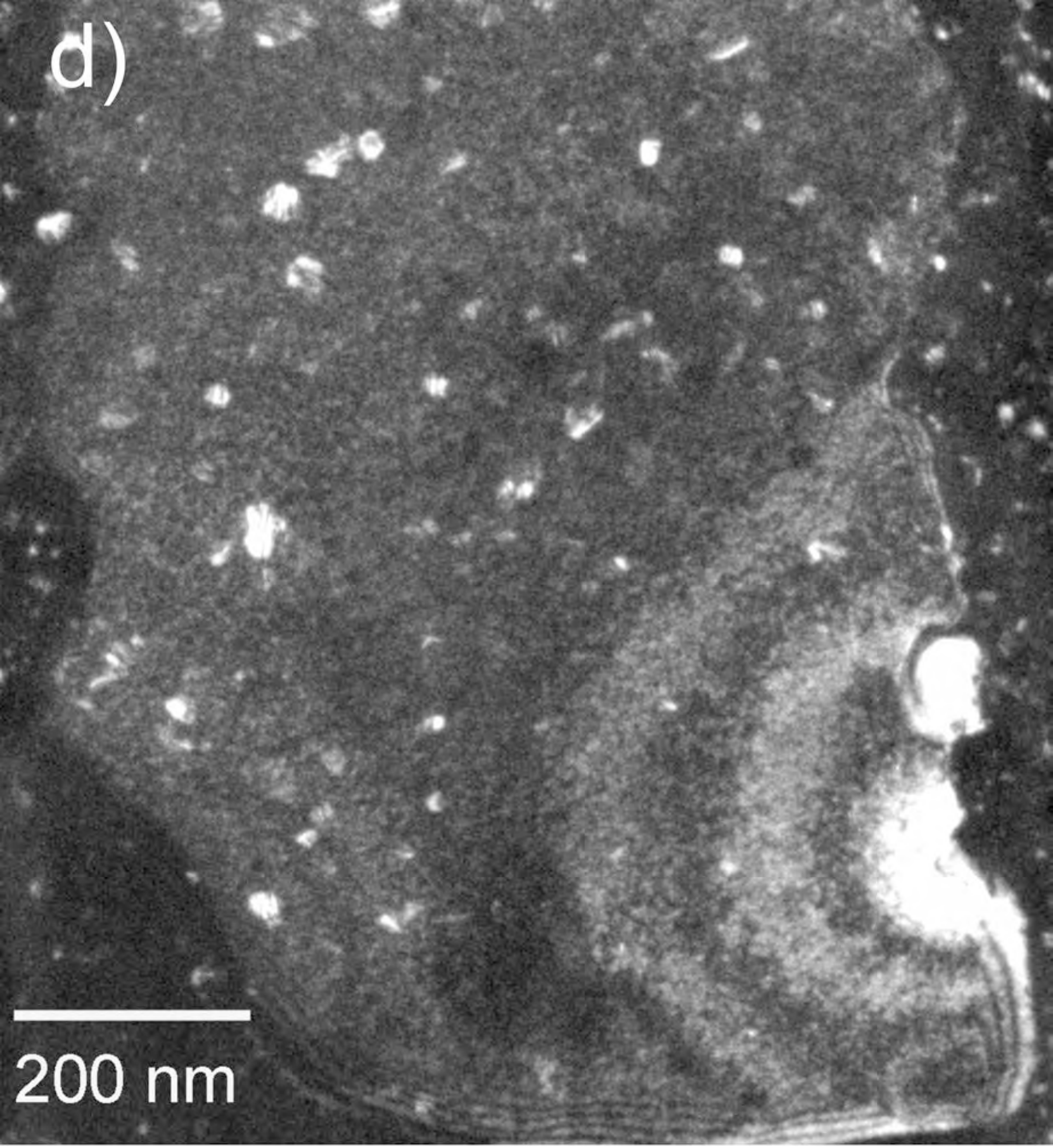

Figure 7d

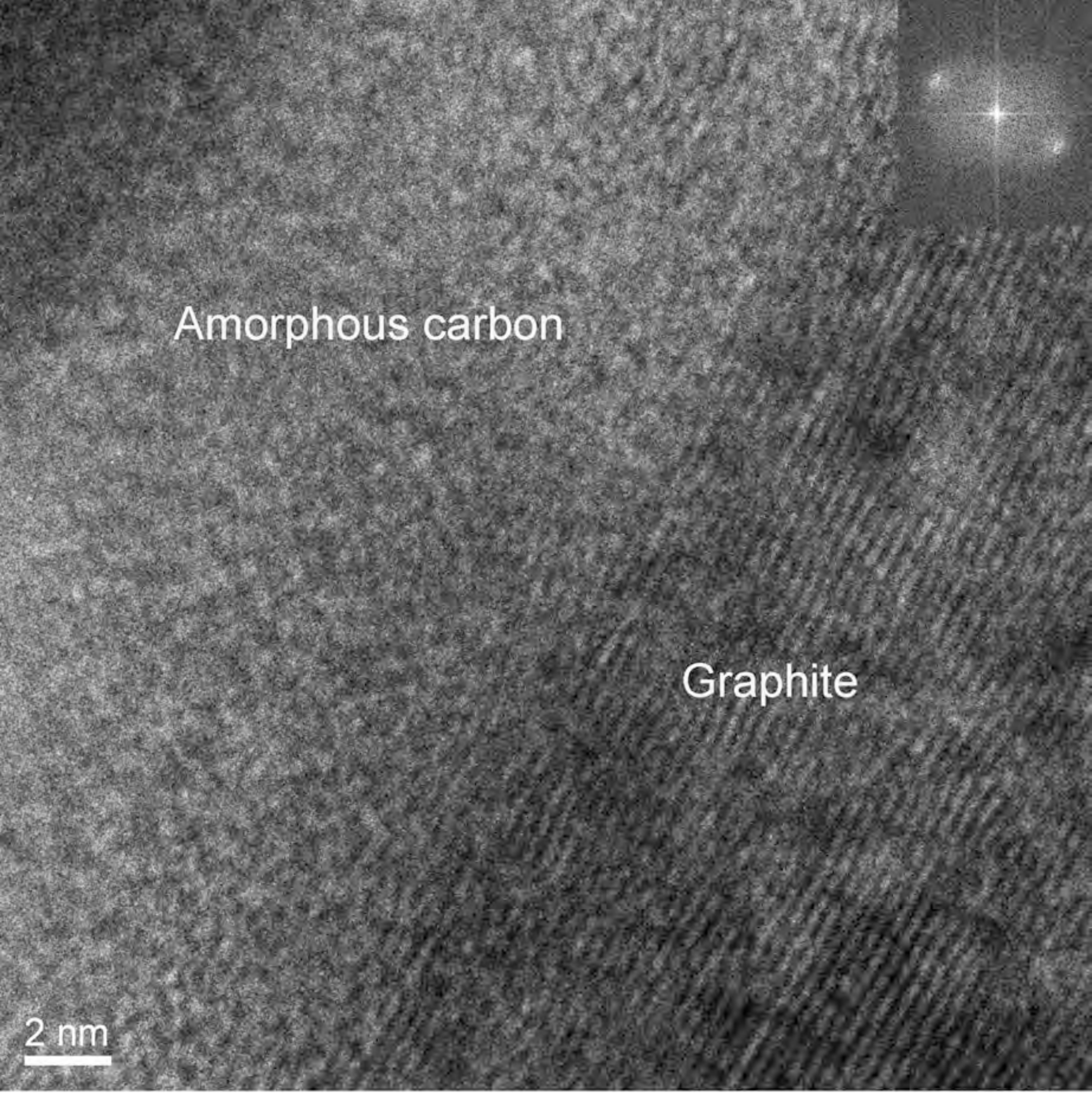

Figure 8

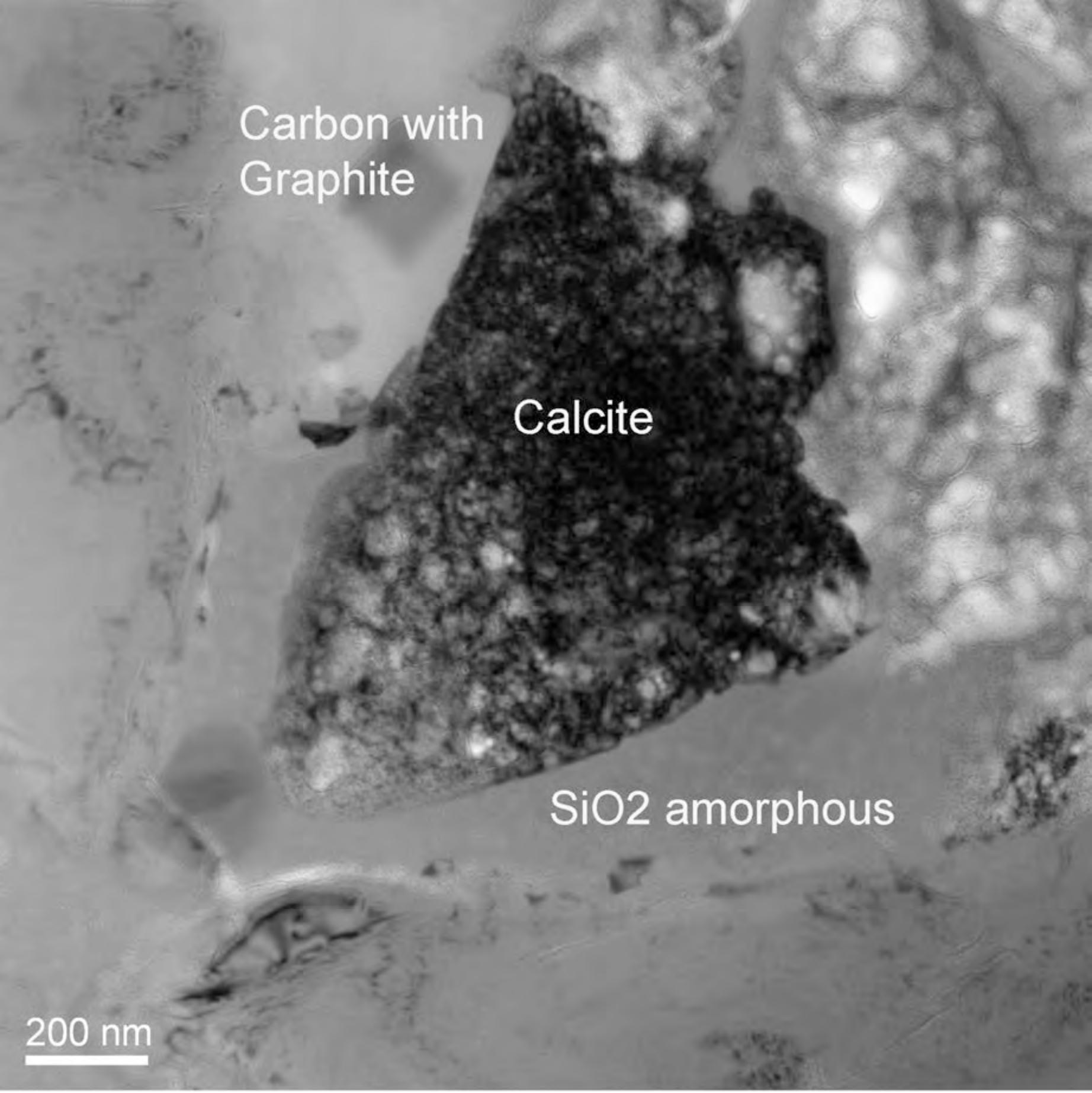

Figure 9